Parkinson's-Linked Synaptojanin 1 Loss in Dopamine Neurons Triggers Synaptic Degeneration and Striatal TH Interneuron Compensation

Youneng Lin[1,#], Bandhan Mukherjee[1,#,†], Man Liu[1,&], Zhaoyan Li[1,&], Xiaoxing Cao[1], Zhen Wang[1] and Mian Cao[1,2,*]

1. Programme in Neuroscience and Behavioural Disorders, Duke-NUS Medical School, Singapore

2. Department of Physiology, National University of Singapore, Singapore

#, &: These authors contributed equally

[†] Present address: Department of Neuroscience, Johns Hopkins University School of Medicine, Baltimore, MD 21205, USA

* Corresponding Author

Contact Information: mian.cao@duke-nus.edu.sg

Abstract

Synaptic dysfunction is an early feature of Parkinson's disease (PD). Synaptojanin 1 (SJ1), a phosphoinositide phosphatase linked to early-onset Parkinsonism (EOP), is essential for synaptic vesicle recycling. To elucidate SJ1's specific role in dopamine (DA) neurons, we generated conditional SJ1 knockout (SJ1-DA cKO) mice. Complete loss of SJ1 resulted in severe, widespread dystrophy of striatal DA terminals, impaired DA metabolism and release, indicating SJ1 has a cell-autonomous role in synaptic transmission across midbrain DA subtypes. Under chronic DA deficiency, SJ1-DA cKO mice exhibited reduced basal locomotor activity but exaggerated amphetamine-induced hyperlocomotion, without obvious deficits in motor coordination. Notably, we observed robust emergence of striatal induced tyrosine hydroxylase-positive interneurons (iTHINs), which expressed multiple DA markers and formed connections with degenerating DA terminals, suggesting local adaptive plasticity. This developmental adaptive response was limited when SJ1 was acutely deleted in adult or aged DA neurons. Our findings highlight SJ1's essential role in DA synapse maintenance and identify a compensatory mechanism that may inform future strategies for PD intervention.

Introduction

Parkinson's disease (PD) is the second most common neurodegenerative disorder, primarily affecting movement. The pathological hallmarks of PD include the selective loss of dopamine (DA) neurons in the substantia nigra pars compacta (SNc) and DA deficiency in the striatum.

Although over 90% of PD cases are sporadic, recent genetic studies have identified more than 20 risk genes and 90 genomic risk loci associated with both familial and sporadic PD(Bandres-Ciga *et al*, 2020). Several of these genes regulate endocytic trafficking at presynaptic terminals, suggesting that impaired synaptic vesicle (SV) recycling is an early pathological feature of PD(Ng & Cao, 2024). A major SV recycling pathway involves clathrin-mediated endocytosis (CME), in which Synaptojanin 1 (SJ1), a lipid phosphatase, plays a crucial role(Saheki & De Camilli, 2012). SJ1 facilitates clathrin uncoating by dephosphorylating PI(4,5)P_2 on the plasma membrane and releasing clathrin adaptors. In its absence, clathrin-coated vesicles (CCVs) accumulate at synapses, as demonstrated in multiple model organisms(Hayashi *et al*, 2008; Milosevic *et al*, 2011; Schuske *et al*, 2003; Verstreken *et al*, 2003).

A homozygous missense mutation (R258Q) in SJ1 has been previously identified in early-onset Parkinsonism (EOP), establishing SJ1 as the PARK20 gene(Krebs *et al*, 2013; Quadri *et al*, 2013). This mutation inactivates the Sac phosphatase domain, resulting in partial loss-of-function (LOF). Since then, additional SJ1 mutations have been linked to Parkinsonism and epilepsy, most of which are homozygous missense or nonsense mutations(Lesage *et al*, 2021; Ng & Cao, 2024). A strong genotype-phenotype correlation exists, where nonsense mutations causing premature truncation in the homozygous state led to severe neurodegeneration, seizures, and early mortality(Dyment *et al*, 2015; Hardies *et al*, 2016). In contrast, homozygous or compound heterozygous missense mutations are associated with milder phenotypes, including Parkinsonism and seizure susceptibility(Lesage *et al.*, 2021; Rauschendorf *et al*, 2017).

More recently, rare heterozygous SJ1 variants have been implicated in EOP, and Sac domain variants have been linked to sporadic PD(Senkevich *et al*, 2024). Additionally, a novel expression quantitative trait locus (eQTL) connection between rs10847864 and SJ1 was identified, highlighting convergence between familial and Genome-Wide Association Study (GWAS) studies(Farrow *et al*, 2022). Furthermore, SJ1 expression is reduced in blood and postmortem PD brain tissues, suggesting it may serve as a biomarker for sporadic PD(Gao *et al*, 2020).

Multiple mouse models have been developed to study SJ1 LOF. Complete SJ1 loss in constitutive homozygous knockout (KO) mice results in early mortality and severe epilepsy, mirroring human patients with homozygous nonsense mutations(Cremona *et al*, 1999; Dyment *et al.*, 2015). Aged SJ1-haploinsufficient (+/-) mice show PD-like features, including alpha-synuclein accumulation, autophagy defects, and DA terminal degeneration(Pan *et al*, 2020). They also exhibit impaired astrocytic glucose sensing and lysosomal dysfunction in midbrain neurons(Pan *et al*, 2021; Zhu *et al*, 2023).

Our previously generated SJ1 knock-in (KI) mice carrying the R258Q mutation (SJ1-KI^{RQ}) exhibit neurological symptoms reminiscent of EOP, including early-onset epilepsy and motor coordination deficits(Cao *et al*, 2017). These mice display generalized synaptic endocytic defects and selective synaptic degeneration in a subset of DA neurons in nigrostriatal pathway, a hallmark of PD pathology(Cao *et al.*, 2017). Additionally, we demonstrated a synergistic interaction between SJ1 and auxilin (PARK19), another PD-linked clathrin uncoating protein(Ng *et al*, 2023). Auxilin-KO mice exhibit dystrophic nigrostriatal DA terminals similar to SJ1-KI^{RQ} mice. In double mutant (Aux-KO/SJ1-KI^{RQ}) mice, lifespan is dramatically reduced, and synaptic endocytic defects and striatal dystrophic changes are exacerbated, further supporting the vulnerability of nigrostriatal neurons to synaptic endocytic impairments(Ng *et al.*, 2023).

Synergistic effects of SJ1 with other PD-linked proteins have also been demonstrated in double mutant mouse models. INPP5F/Sac2, a PI4P phosphatase involved in endosomal trafficking, has been identified as a PD risk gene through GWAS(Nalls *et al*, 2014). Sac2-KO/ SJ1-KI^{RQ} mice show shortened lifespan, more severe endocytic defects, and earlier DA terminal dystrophy(Cao *et al*, 2020). In addition, combining SJ1 heterozygosity with LRRK2 G2019S worsens DA release deficits and motor impairments in aged mice(Pan *et al*, 2017).

While these mouse models have provided valuable insights into SJ1 function in PD, they are all constitutive whole-body mutants, leading to complex behavioral phenotypes and even early death due to global SJ1 loss in the brain. To better delineate SJ1's role in DA neurons in PD, we generated novel DA neuron-specific SJ1 conditional KO models (both genetic and acute deletions) in this study. Complete SJ1 loss in DA neurons of genetic cKO mice results in severe DA terminal dystrophy and DA deficiency throughout the striatum. These mutant mice exhibited reduced spontaneous locomotor activity but showed a marked increase in amphetamine-induced locomotion, likely due to enhanced sensitivity of downstream DA receptors. However, no obvious motor coordination deficit was detected. Notably, we observed a robust increase in striatal tyrosine hydroxylase-positive interneurons (THINs).

These induced THINs acquire DA-like properties and form new connections with DA terminals, suggesting a local compensatory adaptation to DA loss. Furthermore, acute deletion of SJ1 in adult or aged DA neurons triggers similar DA terminal pathology but with minimal adaptive compensation from iTHINs. Our study not only reinforces the critical role of SJ1 in DA synaptic transmission but also offers insight to striatal adaptive plasticity, which if pharmacologically enhanced, might delay or mitigate PD.

Results

Generation of DA-specific SJ1 conditional knockout (cKO) mice genetically

Given that conventional SJ1 KO mice exhibit perinatal lethality within 24 hours of birth, we generated SJ1 flx/flx mice by inserting loxP sites flanking exon 4 of *Synj1* gene using CRISPR/Cas9. These mice were then crossed with the DAT-IRES-Cre line to create DA-specific SJ1 conditional KO mice (DAT-Cre;SJ1 flx/flx), hereafter referred to as SJ1 cKO^{DAT} (Fig. 1A, S1A).

To confirm successful recombination, we performed immunohistochemistry (IHC) on fixed frozen brain sections using antibodies against SJ1 and DA marker tyrosine hydroxylase (TH). In SJ1 cKO^{DAT} mice, SJ1 protein was selectively depleted in TH-positive DA neurons in the SNc and ventral tegmental area (VTA), while SJ1 expression in TH-negative neurons and non-DA brain regions, such as the hippocampus, remained intact (Fig. 1B). These findings confirm efficient and specific KO of SJ1 in DA neurons. SJ1 cKO^{DAT} mice survived into adulthood without seizures, suggesting that epilepsy reported in SJ1-KI^{RQ} mice and constitutive SJ1 KO mice is likely due to SJ1 loss in other brain regions, such as the hippocampus and cortex(Cao *et al.*, 2017; Cremona *et al.*, 1999).

DA Terminal Pathology and DA Deficiency in SJ1 cKO^{DAT} Striatum

To investigate DA-specific pathology in SJ1 cKO^{DAT} mice, we performed IHC for DA-related markers in both midbrain (DA soma) and striatum (DA terminals). In the midbrain, TH-positive DA neurons appeared morphologically intact, with no significant loss of DA neurons in either the SNc or VTA at 2-3 months old and 6-8 months old (Fig. S1B). However, in the striatum, we observed numerous dopamine transporter (DAT) positive dystrophic clusters in SJ1 cKO^{DAT} but not in the control (Fig. 1C, 1D). Consistent with previous study (Cao *et al.*, 2017; Ng *et al.*, 2023), this striatal pathology emerged as early as three weeks after birth, progressively increasing in size and number, and peaking at 2–3 months of age (Figure S1C). Importantly, this pathology was present throughout the striatum, including the dorsal

and ventral striatum, with a higher average number of clusters observed in the nucleus accumbens (NAc) core (Fig. S1D, S1F). This contrasts with SJ1-KI^{RQ} mice (Cao *et al.*, 2017), where dystrophic DA terminals were primarily restricted to the dorsal striatum (nigrostriatal pathway) (Fig. S1D). The widespread pathology observed in the striatum suggests that the complete loss of SJ1 affects striatal DA terminals innervated from both SNc and VTA DA neurons. In contrast, TH-positive DA fibers in the prefrontal cortex (PFC), corresponding to the mesocortical pathway (VTA->PFC) remained unaffected (Fig. S1G). Together, the results from SJ1-KI^{RQ} and SJ1 cKO^{DAT} mice indicate that the loss of SJ1 in DA neurons is sufficient to cause DA terminal dystrophy in a cell-autonomous and gene-dosage dependent manner.

Further characterization showed that these dystrophic clusters were immunopositive for several other DA markers, including TH, aromatic L-amino acid decarboxylase (AADC), vesicular monoamine transporter 2 (vMAT2), and synaptic vesicle glycoprotein 2C (SV2C) (Fig. 1E, S2A). Partial colocalization with general synaptic markers such as synaptotagmin-1 (Syt1) and α-synuclein was observed (Fig. S2B, S2C). In contrast, the pathological form of α-synuclein (pSer129-α-syn) was not detected (Figure S2D). These dystrophic clusters lacked colocalization with D2 dopamine receptors (D2R) or the medium spiny neuron (MSN) marker Darpp32, indicating that the pathology is restricted to DA terminals (Fig. S2E, S2F). Moreover, immunostaining with microglial marker, ionized calcium-binding adapter molecule (Iba1), and astrocyte marker, glial fibrillary acidic protein (GFAP), did not reveal any obvious gliosis and inflammation in the striatum (Fig. S2G, S2H).

Interestingly, these clusters were also negative for clathrin-dependent endocytic proteins either (e.g., clathrin light chain, endophilin 1, and amphiphysin 1), suggesting that a clathrin-independent mechanism may contribute to DA terminal dystrophy (Fig. S3A-S3D). Indeed, electron microscopy (EM) of the SJ1 cKO^{DAT} striatum revealed multilayered, whirl-like membrane structures, similar to those previously observed in SJ1-KI^{RQ} and Auxilin-KO mutant mouse models (Figure 1F) (Ng *et al.*, 2023). These membrane accumulations correlate with DA marker protein clusters and likely reflect abnormal plasma membrane invaginations at DA terminals. They envelop various organelles, including SVs, mitochondria, autophagosomes, and endo/lysosomes (Fig. 1F, S4A-S4B). Notably, no clathrin-coated vesicles (CCVs) accumulation was observed.

We further performed western blot analysis to assess potential changes in DA-related, synaptic and endocytic protein levels in striatal tissue (Fig. 2A, 2B). The analysis revealed a significant reduction in DAT and vMAT2 levels, while TH, AADC and SV2C levels were not significantly altered, suggesting impaired presynaptic DA transmission in SJ1 cKO^{DAT} mice.

The levels of clathrin-associated endocytic proteins—including SJ1, auxilin, BIN1, endophilin 1, dynamin, and AP2, showed no significant changes. Similarly, the level of general synaptic markers such as synapsin, synaptophysin and synaptogyrin 3 were unchanged.

To assess DA metabolism and homeostasis, we conducted high-performance liquid chromatography (HPLC) on striatal extracts from both 2-3 and 6-8 months old SJ1 cKO^{DAT} mice. DA levels were significantly reduced at both time points, whereas DA metabolites, DOPAC (statistically not significant) and homovanillic acid (HVA) levels were elevated (Fig. 2C, 2D). These changes could be a result from impaired SV recycling, reduced vesicular sequestration, and enhanced degradation/oxidation of cytosolic DA.

Following this DA deficiency, we investigated whether SJ1 cKO^{DAT} mice exhibit impaired DA release. To test this, we incubated acute striatal slices with 2 conditions: 40mM potassium chloride (KCl) to depolarize the plasma membrane and evoke vesicular DA exocytosis (Fig. 2E), or with 10 µM amphetamine (AMPH) to induce DA release via DAT-mediated cytosolic DA efflux (Fig. 2F). Under both conditions, DA release was significantly lower in SJ1 cKO^{DAT} mice compared to controls (Fig. 2G, 2H). Reduced KCl-evoked DA release is consistent with the impaired SV recycling and DA package due to reduced vMAT2. Meanwhile, reduced AMPH-induced DA release is likely a result from DAT downregulation, which may limit the action of AMPH, and potentially also reduced cytosolic DA availability due to accelerated degradation.

SJ1 cKO^{DAT} mice Displayed Altered Locomotion without Obvious Motor Coordination Deficits

The strong DA terminal pathology and DA deficiency prompted us to examine the motor function of SJ1 cKO^{DAT} mice. In a 15 min open field test, SJ1 cKO^{DAT} mice showed significant decrease in total distance at both 2-4 and 6-8 months age, suggesting their basal locomotion or exploratory activity is reduced (Fig. 3A, 3B). Given the observed impairment in AMPH-induced DA release, we administered AMPH (3mg/kg) and recorded locomotion for 60 min to test for behavioral alterations. Unexpectedly, SJ1 cKO^{DAT} mice displayed significant increase in total traveled distance compared to controls for both 2-4 and 6-8 months age groups (Fig. 3C, 3D). The representative activity trace (Fig. 3E) and the increase in normalized average traveled distance, expressed as percent of baseline (Fig. 3F, 3G), reflect a markedly heightened response to AMPH treatment. This exaggerated hyperlocomotion in SJ1 cKO^{DAT} mice, despite impaired DA release, suggests a dysregulated DA system, likely driven by downstream signaling or receptor sensitivity.

To explore DA receptors' responses, we performed the open field tests on the mice injected with either D1R agonist (SKF81297 2.5mg/kg) or D2R agonist (quinpirole 0.2mg/kg) to activate them respectively. As shown in Fig 2H-2K, SJ1 cKO^{DAT} mice showed further increased hyperlocomotion after D1R agonist treatment, while the hypolocomotion induced by D2R agonist was comparable to the controls. These results suggest that D1R sensitivity is enhanced in the striatum of SJ1 cKO^{DAT} mice, potentially as a compensatory response to DA deficiency.

To further assess specific motor coordination, we performed the rotarod and balance beam tests. Surprisingly, unlike SJ1-KI^{RQ} mice which showed strong motor coordination deficits, SJ1 cKO^{DAT} mice performed normally on both tasks (Fig. 3L, 3M). These results indicate either the observed DA terminal pathology is insufficient to impair coordination, or compensatory mechanisms may help maintain motor function.

Locally Adaptive induced TH-positive Interneurons (iTHINs) in SJ1 cKO^{DAT} Striatum

In addition to the TH/DAT-positive dystrophic clusters in DA terminals, there was a striking increase in TH-positive neurons within the striatum of SJ1 cKO^{DAT} mice (Fig. 4A). Striatal TH-positive neurons have been reported in rodents(Ibáñez-Sandoval *et al*, 2010; Nakahara *et al*, 2001; Tashiro *et al*, 1989), primates(Betarbet *et al*, 1997; Dubach *et al*, 1987), and humans(Cossette *et al*, 2005; Huot *et al*, 2006; Porritt *et al*, 2000). Previous studies using TH-EGFP mice identified them as TH-positive interneurons (THINs), typically undetectable by IHC in wild-type (WT) mice due to low TH expression masked by dense DA axons(Xenias *et al*, 2015). In SJ1 cKO^{DAT} mice, however, the strong TH protein signal led us to define them as induced TH-positive interneurons (iTHINs). These iTHINs appeared in both dorsal and ventral striatum (Fig. S5A), reaching approximately 200 neurons per coronal section (Fig. 4B). Their emergence paralleled DA terminal dystrophy—first detectable at 3 weeks, peaking at 2–3 months, and persisting into adulthood and aging (Fig. S5B). Since SJ1 deletion is restricted to midbrain DA neurons, this suggests a robust and sustained local adaptation in the striatum.

In the striatum, 95% of neurons are MSNs. In addition, there are several other striatal interneurons, including neuropeptide Y (NPY), parvalbumin (PV), Calretinin-positive GABA interneurons and choline acetyltransferase (ChAT)-positive cholinergic interneurons(Tepper *et al*, 2018). To determine the identity of iTHINs, we performed double staining of TH with specific markers for different neuronal types. As shown in Fig. S6A-S6C, iTHINs were not positive for NPY, PV and ChAT, suggesting they represent a distinct subtype of interneurons.

We observed few iTHINs occasionally expressed Calretinin or Darpp32 (Fig. S6D, S6E), which is consistent with previous studies and suggest heterogeneity within this population(Darmopil *et al*, 2008; Masuda *et al*, 2011). In addition, we don't see obvious changes of other neuronal types we examined in terms of their number, distribution and marker expression levels. Together, these results further support the specificity of iTHINs induction in response to the loss of SJ1 in DA system**.**

DA-Like Features of iTHINs in SJ1 cKO^{DAT} Striatum

To investigate whether iTHINs adopt DA-like features as a compensatory adaptation, we first assessed their expression of key DA biosynthetic enzymes. Importantly, in addition to TH, which is the first enzyme to convert L-tyrosine to L-DOPA, we observed co-expression of the second enzyme AADC, which further converts L-DOPA to DA. All iTHINs were positive for both TH and AADC, suggesting they possess the molecular machinery for DA synthesis (Fig. 4C).

We next examined the expression of DA transporters: vMAT2 and DAT, which are required for vesicular packaging and reuptake of DA, respectively. Both markers colocalized with TH-positive clusters at dystrophic DA terminals (Fig. 4D, 4E) but were absent from iTHINs somata—although DAT gene expression was detected in these neurons (see Fig. 6F).

Given the known heterogeneity of striatal THINs(Mao *et al*, 2019; Tepper *et al.*, 2018), we explored whether iTHINs exhibit subregional adaptations linked to specific midbrain DA neuron subtypes. We first examined aldehyde dehydrogenase 1A1 (ALDH1A1), a marker of A9 SNc DA neurons, which is the population most vulnerable in PD(Cai *et al*, 2014). As expected, ALDH1A1 labeled ventral-tier SNc neurons in both control and SJ1 cKO^{DAT} mice (Fig. S7A). In the striatum, ALDH1A1-positive fibers aggregated with TH/DAT-positive clusters in the dorsal region of SJ1 cKO^{DAT} mice (Fig. 4F, S7B), indicating dystrophic changes in A9-derived terminals. Notably, iTHINs in this region also expressed ALDH1A1 protein, whereas those in the ventral striatum did not, suggesting region-specific adaptation (Fig. 4G, S7B). We also examined Calbindin, a marker of A10 VTA DA neurons(Anderegg *et al*, 2015). While Calbindin labeled a subset of TH-positive neurons in the VTA (Fig. S7C), it was not expressed in any iTHINs (Fig. S7D). Together, these results show that a subset of iTHINs, particularly in the dorsal striatum, exhibit A9-like molecular feature, potentially reflecting a circuit-specific compensatory response to selective nigrostriatal terminal pathology.

A Second Genetic SJ1 cKO Model (SJ1 cKOTH) Recapitulates DA Terminal Pathology and iTHINs Adaptation

To validate the findings, we generated an independent cell type-specific KO model by crossing SJ1 flx/flx mice with the TH-IRES-Cre line, obtaining SJ1 cKOTH mice (Fig. 5A). While this Cre line also targets TH-positive neurons in other regions (e.g., norepinephrine neurons in the locus coeruleus), our analysis focused on DA neurons in the ventral midbrain and striatum.

As shown in Fig. 5B, SJ1 was selectively and completely depleted in TH-positive DA neurons of the SNc and VTA. No obvious DA soma loss was observed in the midbrain of 2-3 months old mice. However, DA terminals in the striatum displayed the same hallmark pathology seen in SJ1 cKO^{DAT} mice—early-onset (1–2 months) dystrophic clusters positive for DA markers including TH, AADC, DAT, vMAT2, SV2C, and ALDH1A1 (Fig. 5C–5F). These clusters were broadly distributed across the striatum, with ALDH1A1 selectively labeled clusters in the dorsal region (Fig. 5G), further confirming both SNc and VTA DA neurons were affected due to complete loss of SJ1. Importantly, iTHINs were again robustly induced in the striatum, paralleling DA terminal pathology. These iTHINs co-expressed TH and AADC, with dorsal striatal subsets also expressing ALDH1A1 (Fig. 5G, 5H), indicating their DA-like feature.

Collectively, results from both SJ1 cKO^{DAT} and cKOTH models demonstrate that SJ1 loss in DA neurons induces cell-autonomous synaptic pathology, along with the emergence of iTHINs, suggesting a secondary, non-cell-autonomous adaptive response.

iTHINs Derive from a pre-existing pool of WT THINs and Activate DAT gene expression in response to SJ1 loss

We next investigated whether striatal iTHINs observed in the SJ1 cKO models originate from a pre-existing population of THINs. To address this, we genetically labeled original WT THINs by crossing Ai9 reporter mice (Cre-dependent tdTomato expression) with SJ1 cKOTH mice, generating Ai9;SJ1 cKOTH mice (Fig. 6A). This enables tdTomato (tdT) expression in all TH gene expressing cells, including DA neurons in the midbrain and THINs in the striatum. In the midbrain, tdT-expressing neurons colocalized with TH-positive DA neurons (Fig. 6B). In the striatum, we observed numerous tdT-expressing neurons in both Ai9;TH-Cre (control) and Ai9;SJ1 cKOTH mice, representing the total THINs (Fig. 6C). Consistent with prior studies(Ibáñez-Sandoval *et al.*, 2010), these tdT-expressing striatal neurons in control mice were not positive for anti-TH staining, implying that they lacked TH protein (Fig.

6C). In contrast, all iTHINs (TH-positive) in SJ1 cKOTH mice were labeled with tdT and comprised approximately 30% of total tdT-expressing neurons (Fig. 6C, 6D). This supports the idea that a subset of WT THINs were induced to express DA-related proteins following SJ1 loss.

We further examined the Cre-dependent tdT labeling pattern in Ai9;SJ1 cKO^{DAT} mice with its respective control, Ai9;DAT-Cre (Fig. 6A). As expected, DAT-Cre drove tdT labeling in midbrain DA soma and striatal axons in both control and mutant mice (Fig. 6E, 6F). In Ai9;DAT-Cre (control) mice, only DA axons were labeled, reflecting that WT THINs do not normally express DAT gene. However, in Ai9;SJ1 cKO^{DAT} mice, we unexpectedly observed tdT-expressing neurons in the striatum (Fig. 6F). Importantly, nearly all tdT-expressing neurons were TH-positive, suggesting that DAT gene is activated in iTHINs (Fig. 6G). Despite having tdT expression, DAT protein was not detected in these iTHINs, possibly due to post-transcriptional suppression. These findings reinforce the DA-like feature of iTHINs and reveal their transcriptional adaptability to DA neuron dysfunction.

iTHINs Establish Novel Connectivity with DA Neurons in SJ1 cKO Striatum

To further study the potential interactions between DA neurons and the newly emerged iTHINs, we employed an adeno-associated virus (AAV)-based strategy to locally label DA neurons in the ventral midbrain using a Cre-dependent system. We unilaterally injected AAV5-flex-tdTomato into the ventral midbrain of SJ1 cKOTH, SJ1 cKO^{DAT} and respective Cre line controls, TH-Cre and DAT-Cre (Fig. 7A). Four weeks post-injection, TH immunostaining revealed tdT expression in midbrain DA neurons and their striatal projections, confirming successful AAV-mediated expression and diffusion throughout DA neurons (Fig. 7B, 7C).

Surprisingly, in both SJ1 cKOTH and SJ1 cKO^{DAT} mice, we detected tdT-expressing iTHINs in the striatum (Fig. 7C). In SJ1 cKOTH mice, despite TH-Cre driving recombination in all WT THINs, only a subset of TH-positive iTHINs were labeled with tdT (Fig. 7C, 7D). This selective labeling of iTHINs was unexpected given that AAV injection was only delivered in the midbrain. In contrast, direct AAV injection into the striatum labeled both iTHINs and WT THINs randomly in SJ1 cKOTH mice (Fig. S8A, S8B second row). As in other controls, striatal AAV injection labeled WT THINs in TH-Cre but not DAT-Cre mice, and labeled iTHINs specifically in SJ1 cKO^{DAT} mice (Fig. S9B). These results suggest a specific interaction between DA neurons and iTHINs, potentially enabling long-distance material transfer, such as AAV axonal transport and inter-neuronal spreading.

To further trace the connectivity between DA neurons and iTHINs, we used a Cre-independent AAV strategy by injecting AAV9-TH-EGFP into the midbrain of B6 control and SJ1 cKO mice (Fig. 7E). In both SJ1 cKO^{TH} and SJ1 cKO^{DAT} mice, EGFP expression was observed in midbrain DA neurons and striatal DA fibers (Fig. 7F, 7G). Again, only a subset of local TH-positive iTHINs expressed EGFP in the SJ1 cKO striatum but not in B6 control (Fig. 7G, 7H). We repeated the AAV9-TH-EGFP midbrain labeling in Ai9;SJ1 cKO^{TH} mice, in which all WT THINs are genetically labeled with tdT (Fig. S8C). EGFP expression was exclusively detected in tdT/TH double positive iTHINs but absent in tdT-positive/TH-negative WT THINs (Fig. S8D), reinforcing the notion of selective connectivity between DA neurons and iTHINs.

Finally, we injected AAV-hSyn-mCherry, driven by a pan-neuronal promoter, into the ventral midbrain of SJ1 cKO mouse models (Fig. 7I). We observed mCherry expression in different neuron types near the injection site, including a subset of TH-positive DA neurons in the midbrain (Fig. 7J). Strikingly, in the striatum of SJ1 cKO—but not WT mice, mCherry-expressing neurons were exclusively iTHINs (anti-TH positive) (Fig. 7K, 7L). In contrast, direct injection of AAV-hSyn-mCherry into WT striatum resulted in random labeling of various local neurons, including Darpp32-positive MSNs and other neuronal types (Fig. S8E, S8F). This result further ruled out the possibility of non-specific AAV leakage from dystrophic DA terminals in SJ1 cKO striatum.

Together, these three independent approaches provide compelling evidence that DA neurons and iTHINs establish a selective and novel connection following SJ1 loss in the DA system.

Upregulation of DA markers in iTHINs distinguishes SJ1 cKO from acute DA lesion mouse models

Previous studies using neurotoxin-induced PD rodent and non-human primate models have shown the increase of THINs in the striatum following DA depletion(Palfi *et al*, 2002; Tande *et al*, 2006; Troshev *et al*, 2023; Ünal *et al*, 2015). To further characterize the iTHINs observed in our genetic SJ1 cKO models, we directly compared them with two acute DA lesion models: (1) the 6-OHDA model and (2) a caspase-3 (Casp3)-mediated ablation model. In the 6-OHDA paradigm, B6 mice received a unilateral injection of the neurotoxin into the midbrain, and brains were collected for IHC analysis two weeks post-injection (Fig. S9A). For the Casp3 lesion model, a Cre-dependent AAV-taCasp3-TEVp was unilaterally injected into the midbrain of DAT-Cre mice, and brain tissue analyzed one-month post-injection (Fig. S9C). In both models, we observed clear evidence of DA neuron degeneration in the

midbrain and a near-complete loss of DA projections in the striatum (Fig. S9B, S9D). Following the depletion of DA fibers, a population of local TH-positive neurons emerged in the striatum (Fig. S9E), consistent with previously reported “THINs”(Xenias *et al.*, 2015). However, compared to the striatum of SJ1 cKO mice, 1) the TH protein expression level is much weaker in these neurons (Fig. S9E, S9F); 2) they did not express other DA-related markers, including AADC and ALDH1A1 (Fig. S9G, S9H); 3) they did not exhibit endogenous DAT gene activity (under the Ai9;DAT-Cre background, Fig. S10A), indicating that iTHINs in SJ1 DA cKO striatum acquire more DA-like features. In Table S1, we summarized the differences between iTHINs in SJ1 DA cKO mice and WT THINs from these two neurotoxin models.

In summary, various labeling strategies revealed that about 30% of the original WT THINs were specifically induced to express DA-like features (TH/AADC protein and DAT gene activity) following DA-specific SJ1 cKO. In these iTHINs, a subset in the dorsal striatum also expressed the A9 DA-specific marker ALDH1A1, matching their nigrostriatal DA input from the midbrain. Furthermore, iTHINs appear to form new and specific connections with dystrophic DA terminals, further supporting a role in adaptive compensation for DA deficiency (Fig. S10B).

Acute SJ1 KO in Adulthood Triggers Similar DA Terminal Pathology with limited Developmental Compensation from iTHINs

As described above, iTHINs in genetic SJ1 cKO mice begin to appear at 2-3 weeks of age, peaking at 2-3 months, suggesting that this is an adaptation during early development stage. To bypass this developmental adaption, we generated acute SJ1 KO mice in DA neurons by unilaterally injecting AAV-TH-Cre virus into the ventral midbrain of adult (2-month) or aged (12-month) SJ1 flx/flx mice (Fig. 8A). To assess the potential non-specific toxic effect of AAV-Cre expression in DA neurons(Erben *et al*, 2022; Rezai Amin *et al*, 2019), we performed parallel injections in WT mice and found no loss of DA somata or fibers (Fig. S11A, S11B).

At 3-4 months post AAV injection, we confirmed successful acute KO of SJ1, observing efficient depletion of SJ1 in most TH-positive DA neurons on the ipsilateral midbrain (Fig. 8B). Immunostaining results revealed numerous TH/DAT-positive clusters throughout the striatum, resembling the DA terminal pathology observed in genetic SJ1 cKO mice (Fig. 8C, 8D). This confirms the synaptic defects across the entire DA population projecting to the striatum due to the complete loss of SJ1. Importantly, even though the number and density of DA terminal clusters were comparable to those observed in genetic SJ1 cKO mice, very

few TH-positive iTHINs were detected—about 10% of the number observed in genetic SJ1 cKO mice (Fig. 8E, 8F). Our findings suggest that the secondary compensatory response from iTHINs is primarily induced during early development to compensate for DA terminal defects. Future longitudinal studies are needed to determine whether acute SJ1 loss leads to progressive DA neurodegeneration and motor deficits via axonal die-back.

Discussion

In this study, we examined the consequences of SJ1 loss in DA neurons using newly generated DA-specific SJ1 cKO mice. We identified two major cellular outcomes: (1) a primary defect marked by severe dystrophy of DA terminals, with accumulation of DA markers and excess membranes in both dorsal and ventral striatum; and (2) a localized adaptive response involving a robust increase in DA-like striatal TH-positive interneurons (iTHINs), which were found to form selective connections with DA terminals. Comparative analysis with acute adult SJ1 deletion and other lesion models indicates that this iTHINs induction is specific to early developmental loss of SJ1. This adaptive striatal plasticity may serve as an early neuroprotective mechanism to maintain DA homeostasis or delay terminal degeneration, offering a potential therapeutic strategy to preserve DA function in PD.

Cell-Autonomous, Clathrin-Independent Role of SJ1 in the Neuromodulatory System

SJ1 has been extensively studied in excitatory and inhibitory synapses, where it plays a key role in clathrin uncoating during clathrin-mediated SV endocytosis and recycling. Constitutive whole-body SJ1 KO mice die postnatally with severe epilepsy, suggesting imbalanced excitatory/inhibitory transmission during development(Cremona *et al.*, 1999). While DA-specific SJ1 cKO mice survive to adulthood without seizures, our findings show that striatal DA terminals from both the SNc and VTA undergo significant dystrophic changes, indicating a cell-autonomous role for SJ1 in regulating DA synaptic function. Interestingly, no accumulation of endocytic proteins involved in CME or CCVs were detected in these dystrophic terminals. As neuromodulators, DA neurons release transmitters via "volume transmission", a slower process that does not rely on precise synaptic contact sites(Özçete *et al*, 2024). This contrasts with the fast "synaptic transmission" seen in excitatory and inhibitory synapses, which primarily recycle SVs through CME. Given these differences, it is plausible that DA synapses utilize alternative mechanisms for SV recycling, such as bulk endocytosis (Chanaday *et al*, 2019).

In addition to DA, another neuromodulator norepinephrine neurons are also vulnerable in PD, likely due to shared features such as pace-making firing, extensive axonal arborization, and

accumulation of cytosolic oxidized catecholamines. Future studies using our cell type specific SJ1 cKO model could determine whether SJ1 similarly regulates SV recycling in norepinephrine neurons and how its dysfunction contributes to their selective degeneration in PD.

Gene Dosage-Dependent SJ1 Loss Correlates with the Severity of DA pathology

There is a clear genotype-phenotype correlation in SJ1-linked PD cases, which is mirrored in mouse models carrying different SJ1 mutations. DA pathology in these models also reflects SJ1 gene dosage. The SJ1-KI^{RQ} model shows selective degeneration of nigrostriatal terminals, while the SJ1 cKO model exhibits more widespread DA terminal dystrophy. This indicates that both A9 and A10 DA neurons are susceptible to impaired SJ1-mediated SV recycling, with A9 SNc neurons being particularly vulnerable, even with partial SJ1 loss. A similar synergistic effect is seen in the Auxilin KO/SJ1-KI^{RQ} double mutant, which displays more severe DA terminal pathology than either single mutant(Ng *et al.*, 2023). More recently, SJ1 haploinsufficiency has been linked to abnormal mesolimbic signaling and mild motivational deficits(Mejaes *et al*, 2024), suggesting a broader role for SJ1 in VTA DA function that can be further explored using our SJ1 DA cKO mice. Together, these findings highlight impaired SV recycling as a key driver of DA dysfunction, with partial impairment leading to selective degeneration of SNc DA terminals as a hallmark of PD pathogenesis.

Altered Locomotor Activity but No Obvious Coordination Deficits in SJ1 DA cKO mice

Along with severe DA terminal pathology, the striatum of SJ1 cKO mice showed reduced DA content, increased breakdown, and impaired DA release/efflux. The reduced spontaneous locomotion in the open field likely reflects this diminished DA tone. However, the exaggerated hyperlocomotion after AMPH treatment, despite having blunted AMPH-induced DA efflux, points to compensatory postsynaptic hypersensitivity. Consistently, SJ1 cKO mice exhibited a significant increase in locomotion after D1R, but not D2R agonist treatment, suggesting the hypersensitization of DA receptors in the striatum.

Surprisingly, SJ1 cKO mice displayed intact motor coordination in rotarod and balance beam tests, despite showing more severe pathology than SJ1-KI^{RQ} mice. This preservation suggests several possibilities: (1) motor symptoms in SJ1-KI^{RQ} mice may arise from combined SJ1 dysfunction across multiple brain regions, not just DA neurons; (2) DA terminal dystrophy observed in SJ1 mutant mice may represent a prodromal phase of PD that does not progress to full clinical manifestations within the mouse lifespan; and (3) local

compensatory mechanisms within the striatum may preserve basic motor coordination despite significant synaptic dysfunction.

Our findings align with recent studies using DA-specific cKO mouse models of two important synaptic transmission proteins: the Ca^{2+} sensor Syt1 and the release site organizer RIM1/2(Cai *et al*, 2024; Delignat-Lavaud *et al*, 2023). In both cKO models, although activity- or action potential-induced phasic DA release is significantly abolished, the mice do not exhibit obvious motor defects(Cai *et al.*, 2024; Delignat-Lavaud *et al.*, 2023). Furthermore, early compensatory changes, such as receptor adaptation and enhanced DA synthesis, packaging, and innervation, have been observed in the striatum of Syt1 DA-cKO mice(Delignat-Lavaud *et al.*, 2023). These results suggest that DA-dependent motor functions can be sustained by basal extracellular DA levels and striatal compensatory plasticity.

Taken together, the converging results from three DA-specific cKO models with impaired synaptic transmission support the idea that strong motor coordination deficits of PD only emerge after extensive DA denervation. These models may therefore capture key aspects of the pre-symptomatic or early compensatory stages of PD, where functional abnormalities in DA terminals are present, but motor coordination remain intact.

Adaptive Compensation of iTHINs in SJ1 DA cKO Striatum

DA-like Features of iTHINs

A prominent adaptive change in SJ1 DA cKO mice is the robust increase in iTHINs, accounting for approximately 30% of the original total THINs population in the striatum. A much milder induction of iTHINs was also observed in SJ1-KI^{RQ} and Auxilin KO/SJ1-KI^{RQ} double mutants, suggesting that this response is specific to endocytic defects and modulated by gene dosage(Ng *et al.*, 2023).

Neurotoxin-induced PD models (6-OHDA, MPTP) in rodents and non-human primates have shown increased THINs in the striatum following DA depletion, suggesting a potential compensatory or protective role(Palfi *et al.*, 2002; Tande *et al.*, 2006; Troshev *et al.*, 2023; Ünal *et al.*, 2015). However, it remains debatable whether these THINs qualify as bona fide DA neurons capable of expressing key DA markers (e.g., AADC, DAT) and producing/releasing DA(Troshev *et al*, 2022; Troshev *et al.*, 2023; Xenias *et al.*, 2015).

In our study, when compared with acute 6-OHDA and Casp3 lesion models, iTHINs in SJ1 cKO mice displayed distinct DA-like features: strong co-expression of TH and AADC, activation of the DAT gene, and expression of the SNc DA neuron marker ALDH1A1 in a subset of dorsal striatal iTHINs. While SV-related markers like vMAT2 were not detected, it's worth noting that non-vesicle mediated somato-dendritic DA release in the midbrain has been proposed previously(Rice *et al*, 2011). Future biochemical and physiological studies are needed to determine iTHINs capacity for DA production and release. Alternatively, iTHINs may retain their GABAergic interneuron identity and contribute to striatal homeostasis by modulating local circuitry(Xenias *et al.*, 2015).

Crosstalk Between iTHINs and Dystrophic DA Terminals in SJ1 cKO Striatum

Our data also reveal a previously unrecognised form of striatal circuit plasticity involving long-distance communication between DA neurons and iTHINs. First, the enrichment of iTHINs expressing A9 SNc DA marker ALDH1A1 in the dorsal striatum indicates a region-specific and circuit-dependent compensatory response to DA terminal degeneration. Second, AAV-based tracing from SJ1 KO DA neurons resulted in selective co-labeling of striatal iTHINs, strongly suggesting material transfer or spreading from degenerating DA terminals. The exact pathway for this connection remains elusive but may involve newly formed synapses or non-synaptic mechanisms such as exosomes or tunneling nanotubes that should be explored in future studies(Ramírez-Jarquín *et al*, 2022; Rufino-Ramos *et al*, 2023).

A key open question is what signal striatal WT THINs detect to initiate their induction. While extracellular DA levels were previously shown to negatively regulate THINs number(Busceti *et al*, 2012), intriguingly, acute DA lesion models with severe DA depletion do not induce iTHINs. This indicates that other factors—likely released from DA fibers—are required to initiate and sustain DA-like features in iTHINs. The observation that acute SJ1 loss in adult or aged DA neurons significantly reduces the number of iTHINs further implies that this signal diminishes with age and is restricted to early developmental window.

Moreover, prior studies have demonstrated that THINs form connections with other striatal neurons(Ibáñez-Sandoval *et al.*, 2010; Tepper *et al.*, 2018), making it plausible that iTHINs actively engage in local crosstalk. Advanced approaches including single-nucleus RNA sequencing and spatial transcriptomics could be employed to further study the molecular identity and functional role of iTHINs in striatal microcircuits. By elucidating these mechanisms of striatal plasticity, we can open new paths for therapeutic strategies that target circuit-level compensation in PD.

Methods and Materials

Animals

Mice were housed in SPF rooms with a 12-hour light/dark cycle. All experiments involving animals were conducted according to the protocol approved by SingHealth Institutional Animal Care and Use Committee (IACUC).

SJ1-KI^{RQ} mouse line was generated as described before and a gift from Prof Pietro De Camili (Yale University)(Cao *et al.*, 2017). SJ1 flx/flx (C57BL/6J-Synj1^{em1cyagen}; S-CKO-00357, Cyagen) was generated by inserting loxP sites flanking exon 4 of Synj1 using CRISPR/Cas9. These mice were crossed with DAT-IRES-Cre (C001024, Cyagen) and TH-IRES-Cre knock in line (EM:00254, European Mouse Mutant Archive; kindly provided by Dr Sarah Luo, IMCB-A*STAR) to obtain double heterozygous, +/DAT-Cre;SJ1 +/flx and +/TH-Cre;SJ1 +/flx mice, respectively. To create DA-specific SJ1 conditional KO mice, double heterozygous mice were crossed with homozygous SJ1 flx/flx, obtaining +/DAT-Cre;SJ1 flx/flx and +/TH-Cre; SJ1 flx/flx mice, referred to as SJ1 cKO^{DAT} and SJ1 cKOTH, respectively. Appropriate littermate or age-matched controls (SJ1 flx/flx or +/DAT-Cre;SJ1 +/flx or +/TH-Cre;SJ1 +/flx) were used in all experiments. All mice used in the experiments with Cre-dependant promoter were heterozygous, simply referred as DAT-Cre and TH-Cre in the manuscript.

Ai9 mice (B6.Cg-Gt(ROSA)26Sortm9(CAG-tdTomato)Hze/J; RRID:IMSR_JAX:007909) were kindly provided by Prof Enrico Petretto (Duke-NUS) for specific labeling following Cre-mediated recombination. Homozygous Ai9 mice were first crossed with homozygous SJ1 flx/flx to obtain double heterozygous, +/Ai9;SJ1 +/flx mice. Subsequent models involving Ai9 were all heterozygous Ai9, hence simply referred as Ai9 in the manuscript. Ai9;SJ1 +/flx mice were then crossed with SJ1 cKO^{DAT} and SJ1 cKOTH to obtain Ai9;SJ1 cKO^{DAT} and Ai9;SJ1 cKOTH, respectively. Appropriate littermate or age-matched controls were used in all experiments.

For SJ1 acute KO mice model, SJ1 flx/flx mice were employed. Briefly, mice were stereotactic injected AAV.rTH.PI.Cre.SV40 (1ul) (Addgene-#107788) unilaterally in right midbrain (AP 3.3 mm, ML 1.2 mm, DV 4.3 mm) after anesthetized by isoflurane (5% induction, 2% maintenance at 0.5-0.8 L/min oxygen or air flow). Mice brain tissues were harvested for IHC at 3-4 months post injection.

For 6-hydroxydopamine (6-OHDA; H4381, Sigma-Aldrich) lesion model, B6 mice (C57BL/6J; RRID:IMSR_JAX:000664**)** were treated with desipramine (D3900, Sigma-Aldrich; i.p. 25 mg/kg) 30 min prior to 6-OHDA infusions to prevent noradrenergic neurons. 6-OHDA (2.88

ug, dissolved in 0.2% ascorbate/saline solution) was unilaterally pressure injected into the right midbrain (AP 3.3 mm, ML 1.2 mm, DV 4.3 mm). Mice brain tissues were harvested for IHC at 2 weeks post 6-OHDA injection.

For Casp3 ablation model, Cre-dependent virus, pAAV-flex-taCasp3-TEVp (1ul) (Addgene-#45580) were unilaterally injected in Cre heterozygous mice right midbrain (AP 3.3 mm, ML 1.2 mm, DV 4.3 mm) after anesthetizing. Mice brain tissues were harvested for IHC at one month post injection.

AAV Labeling Surgery

Animals were anesthetized using isoflurane (5% induction, 2% maintenance at 0 .5-0.8 L/min oxygen or air flow) and secured in a stereotaxic apparatus. For virus injection, pAAV-FLEX-tdTomato (1ul) (Addgene-#28306), rAAV-mTH-EGFP (BrainCase-#BC-0319) (0.5ul) or pAAV-hSyn-mCherry (Addgene-#114472) (1ul) was infused into the midbrain (targeting the VTA and SNc) and the striatum. The coordinates for the midbrain were AP 3.3 mm, ML 1.2 mm, DV 4.3 mm. For striatal infusion, the coordinates were AP -0.3 mm, ML -2.0 mm, DV -2.5 and -4.0 mm.

Infusions were conducted using a Hamilton syringe (Hamilton-Syringe, NEUROS, 7002, 2UL. The infusion rate for all surgery was 100nl/min, unless stated otherwise. Syringe was left in place for an additional 10 min before withdrawal to prevent retrograde mass flow. All injection procedures were performed on a heating pad (37°C) to maintain body temperature. Following surgery, mice recovered in another clean cage on a heating pad until they were awake.

Antibodies

The antibodies used in this study were obtained from commercial sources as stated: mouse anti-α-synuclein (610786, RRID: AB_2748880), mouse anti-AP2 (611350, RRID: AB_398872) and mouse anti-Dynamin (610245, RRID: AB_397640) from BD Biosciences; goat anti-ChAT (AB144P, RRID: AB_2079751), mouse anti-clathrin light chain (AB9884, RRID: AB_992745), rat anti-DAT (MAB369, RRID: AB_2190413), mouse anti-SV2C (MABN367, RRID: AB_2905667) and rabbit anti-TH (AB152, RRID: AB_390204) from Merck Millipore; mouse anti-β-actin (sc-47778, RRID: AB_2714189) and mouse anti-BIN1 99D (sc-13575, RRID:AB_626753) from Santa Cruz Biotechnology; rabbit anti-ALDH1A1 (HPA002123, RRID: AB_1844722), rabbit anti-GFAP (ZRB2383, RRID: AB_2905668) and rabbit anti-SJ1 (HPA011916, RRID: AB_1857692) from Sigma-Aldrich; rabbit anti-Endophilin 1 (159002, RID:

AB_887757), mouse-anti Calretinin (214111, RRID: AB_2619904), mouse anti-TH (213211, RRID: AB_2636901), rabbit anti-Amphiphysin 1 (120002, RRID: AB_887690), rabbit anti-Synaptogyrin 3 (103302, RRID:AB_2619752), rabbit-anti Synaptophysin 1 (101002, RRID:AB_887905), rabbit anti-AADC (369003, RRID: AB_2620131), guinea pig-anti Calbindin D28k (214005, RRID: AB_2619902), mouse anti-Parvalbumin (195011, RRID: AB_2619883) and rabbit anti-D2R (376 203, RRID: AB_2636918) from Synaptic Systems; rabbit anti-VMAT2 (MSFR106400, RRID: AB_2571857) from Nittobo Medical; rabbit anti-DARPP-32 (2306, RRID: AB_823479) and rabbit anti-Neuropeptide Y (11976, RRID: AB_2716286) from Cell Signaling Technology; rabbit anti-Iba1 (019-19741, RRID: AB_839504) from FUJIFILM Wako Pure Chemical Corporation; goat anti-ALDH1A1 (AF5869_RRID: AB_2044597) from R&D Systems; rabbit anti-alpha synuclein phospho S129 (EP1536Y, RRID:AB_765074) from abcam; mouse anti-GAPDH (60004-1, RRID: AB_2107436) and rabbit anti-GAPDH (10494-1-AP, RRID: AB_2263076) from Proteintech. The rabbit anti-Synapsin was obtained from Prof Pietro De Camilli's lab at Yale University.

Secondary antibodies used were all purchased from commercial sources as stated: donkey anti-mouse IgG (H□+□L) Alexa Fluor Plus 488 (A32766, RRID: AB_2762823), donkey anti-mouse IgG (H□+□L) Alexa Fluor 594 (A21203, RRID: AB_2535789), donkey anti-mouse IgG (H□+□L) Alexa Fluor Plus 647 (A32787, RRID: AB_2762830), donkey anti-rabbit IgG (H□+□L) Alexa Fluor Plus 488 (A32790, RRID: AB_2762833), donkey anti-rabbit IgG (H□+□L) Alexa Fluor Plus 594 (A32754, RRID: AB_2762827), donkey anti-rabbit IgG (H□+□L) Alexa Fluor 647 (A32795, RRID: AB_2762835), donkey anti-rat IgG (H□+□L) Alexa Fluor Plus 488 (A48269, RRID: AB_2893137), donkey anti-rat IgG (H□+□L) Alexa Fluor 594 (A21209, RRID: AB_2535795), donkey anti-goat IgG (H□+□L) Alexa Fluor 488 (A11055, RRID: AB_2534102), donkey anti-goat IgG (H□+□L) Alexa Fluor 594 (A32758, RRID: AB_2762828), goat anti-guinea pig IgG (H□+□L) Alexa Fluor 488 (A11073, RRID: AB_2534117) and goat anti-guinea pig IgG (H□+□L) Alexa Fluor 647 (A21450, RRID: AB_2535867) from Life Technologies; goat anti-mouse IgG light chain HRP (AP200P, RRID:AB_805324) and mouse anti-rabbit IgG light chain HRP (MAB201P, RRID:AB_827270) from Merck; IRDye 800CW donkey anti-rabbit IgG (926-32213, RRID: AB_621848), IRDye 800CW donkey anti-mouse IgG (926-32212, RRID: AB_621847), IRDye 680RD donkey anti-mouse IgG (926-68072, RRID: AB_10953628) and IRDye 800CW goat anti-rat (926-32219, RRID: AB_1850025) from LI-COR Biosciences.

Brain Histology and Immunofluorescence

Mice were anesthetized with a Ketamin/Xylazine anesthetic cocktail injection, perfused transcardially with ice-cold 4% paraformaldehyde in 1 X phosphate-buffered saline (PBS) and the brains were kept in the same fixative overnight at 4°C. On the next day, brains were transferred to 30% sucrose in 1 X PBS and kept overnight at 4°C on top of a roller. Brains were then embedded in OCT (Tissue-Tek) and freeze in liquid nitrogen-cooled 2-methylbutane (Isopentane). Coronal or sagittal sections of 20 µm thickness were cut with a cryostat. The sections were either mounted on adhesive slide, SuperFrost® Plus (VWR) or collected as floating sections in 1 X PBS in a 24-well plate. Sections were then blocked in 5% BSA and 0.1% Triton X-100 in 1 X PBS for 1 hour at room temperature. After blocking, sections were incubated with primary antibodies and kept overnight at 4°C. Subsequently, sections were washed 3 times for 10 min with 0.1% Triton X-100 in 1 X PBS, then incubated with Alexa-conjugated secondary antibodies for 1 hour at room temperature. Finally, the sections were mounted with Fluoromount-G (Invitrogen) and sealed with nail polish. The floating sections were mounted onto slides after all the staining procedures. Images were acquired with Andor BC43 (Oxford Instruments) with 10x, 20x and 40x oil objective or a spinning disk system (Gataca Systems) based on an inverted microscope (Nikon Ti2-E; Nikon) equipped with a confocal spinning head (CSU-W, Yokogawa) and a Plan-Apo 20x and 40x oil objective.

For stereological analysis of TH-positive DA neurons in the midbrain, 30 µm coronal section were collected incubated with 0.1% H2O2 for 5 min to quench endogenous peroxidase activity and subsequently incubated with buffer containing 5% BSA, and 0.1% Triton X-100 in 1X PBS for 1 hour at room temperature. Next, sections were incubated overnight at 4°C with anti-TH primary antibody (1:1000). The sections were then washed with 1X PBS three times for 10 min and incubated with a biotinylated anti-rabbit secondary antibody (Vector Laboratories, USA) for 1 hour at room temperature, later followed by incubation with Avidin/Biotin complex (ABC) reagent (Vector Laboratories, USA) at room temperature. Finally, immunoreactivity was revealed by incubation with diaminobenzidine (DAB). Stereological analysis was performed using the optical fractionator probe in the Stereo Investigator (MBF Bioscience) software. A total of 7-9 coronal sections of every fourth sections were collected across the midbrain and used for counting. The SN and VTA regions were outlined based on the Allen mouse brain atlas and counting was performed using 63x oil lens. The parameters used were guard zone of 2 µm, dissector height of 13 µm and counting frame of 200 µm x 200 µm.

Electron Microscopy

2 months old mouse was anesthetized and fixed by transcardial perfusion with 4% paraformaldehyde and 0.125% glutaraldehyde (EMS, Hatfield, PA) in 0.1 M PB buffer. Brain was removed and dissected in small pieces (1 × 1 × 1 mm^3) and further incubated in 2.5% glutaraldehyde in 0.1 M PB buffer at 4 °C overnight. The samples were then washed for 5 min in 1 X PBS for three times. The samples were post-fixed with 1% osmium tetroxide for 1 hour and washed with distilled water. They are then dehydrated through an ethanol series (25%, 50%, 75%, 95% and 100%) and absolute acetone, before infiltrating with araldite resin/acetone mixtures. On the next day, samples were further infiltrated in pure resin at 40°C to 50°C, then embedded in resin and polymerised at 60°C for 24 hours. The embedded sample was sectioned into 100nm slices with a Leica UC6 ultramicrotome and stained with lead citrate. Images were captured with JEOL JEM-1400Flash TEM, operating at 100kV.

Immunoblotting

Striatum tissues were homogenized in buffer containing 20 mM Tris-HCl (pH 7.4), 150 mM NaCl, 2 mM EDTA and cOmpleteTM EDTA-free Protease Inhibitor Cocktail (Roche, USA). The homogenized samples were centrifuged at 700 g for 10 min to obtain the post-nuclear supernatant (PNS). Protein concentration was determined by the Pierce BCA Protein Assay Kit. SDS-PAGE and western blotting were performed by standard procedures. The membranes were blotted with primary antibodies and then IRDye® Secondary Antibodies (LI-COR, USA) or HRP light chain secondary antibodies. The protein bands were detected using Odyssey ® CLx imaging system or Bio-Rad ChemiDoc Touch Imaging System, and its intensity was quantified via Image Studio. A minimum of three independent sets of samples were used for quantification.

HPLC

Striatum tissues dissected from mice brain were homogenized in 0.5 N perchloric acid with 100 µM of deferoxamine mesylate and 100 µM of glutathione. The homogenized samples were further sonicated, centrifuged and the supernatants were filtered using 0.1 µm PVDF centrifugal filters before collecting the filtrates for HPLC analysis. A reversed-phase UltiMate 3000 HPLC system (Thermo Fisher Scientific) with an electrochemical detector and a reversed-phase column (Vydac Denali, C18, 4.6 x 250 mm, 5 µm particle size, 120 Å pore size) were used to run the samples. The HPLC run was performed at a flow rate of 1 ml per minute with a mobile phase containing 1.3% sodium acetate, 0.01% EDTA (pH8.0),

0.5% sodium 1-heptanesulfonate, 7% acetonitrile (v/v) and 2% methanol (v/v), adjusted to pH 4.0 with acetic acid. All buffers used for HPLC analysis were double filtered through 0.2 μM nylon membranes. Dopamine, DOPAC and HVA levels in the samples was identified by retention time of their respective standard and quantified by measuring the area under the peak using the software ChromeleonTM 7.2 Chromatography Data System (Thermo Fisher Scientific). The areas under the peaks were normalized to their respective tissue weight.

Acute Brain Slice Preparation

Mouse brains were rapidly removed after decapitation and placed in high-sucrose ice-cold oxygenated artificial cerebrospinal fluid (ACSF) containing the following (in mM): 125 NaCl, 25 $NaHCO_3$, 10 glucose, 2.5 KCl, 2.5 $MgCl_2$, 0.5 $CaCl_2$, 1.24 NaH_2PO_4, 1.68 HEPES, pH 7.4 and 95% O_2/5% CO_2. Coronal brain slices were cut at a thickness of 250 μm using a vibratome (VT1200S, Leica Biosystems) and immediately transferred to an incubation chamber filled with ACSF containing the following (in mM): 125 NaCl, 25 $NaHCO_3$, 10 glucose, 2.5 KCl, 2 $MgCl_2$, 1 $CaCl_2$, 1.24 NaH_2PO_4, 1.68 HEPES, pH 7.4 (300–310 mOsm), equilibrated with 95% O_2 and 5% CO_2. Slices were allowed to recover at room temperature at least for 60 min.

For KCl-evoked and AMPH-induced release, striatum brain slices were incubated with 300 μL pre-warmed ACSF containing the following (in mM): 125 NaCl, 25 $NaHCO_3$, 1.25 $NaH_2PO_4.2H_2O$, 2.5 KCl, 1.8 $CaCl_2$, 1 $MgCl_2$, 0.4 ascorbic acid, pH 7.4 (300–310 mOsm) at 37 °C, 5 min. The incubation medium in this step served as the baseline control for subsequent measurements. Another 300μL ACSF containing 40 mM KCl or 10 μM amphetamine (AMPH; d-(+)-Amphetamine sulfate, D961, Age D'or) were added to incubated with the same striatum brain slices at 37 °C, 5 min. The incubation medium in this step served as the KCl-evoked or AMPH-induced DA released samples from striatum of control (DAT-Cre/SJ1 +/flx) and SJ1 cKO^{DAT} mice for subsequent HPLC detecting. After adjusting the final concentration of the ACSF buffer to 0.1 N perchloric acid, the DA released samples was filtered through 0.1 μm PVDF centrifugal filters and subjected to HPLC analysis using the same parameters as those used for striatum tissues detection. The areas under the peaks were normalized to their respective protein concentration.

Motor Behavioral Tests

SJ1 cKO^{DAT} and mice between 2-8 months old were used for balance beam and rotarod tests. The mice were divided into two age groups: 2-3 months old (n= 13 for Ctrl, n=15 for SJ1 cKO^{DAT}) and 6-8 months old (n=9 for Ctrl and n=10 for SJ1 cKO^{DAT}). Both males and females were used for the behavioral assays. Both tests were conducted during the light period. The mice were allowed to be acclimatized to the test for at least 30 min before each test.

Balance Beam Test

A narrow beam (10 mm width) was suspended 15 cm above a soft padding. Mice were placed on end of the beam and during their trip towards the other end, the number of missteps (paw slips) was recorded. The test was conducted thrice for each mouse and the average number of missteps was calculated.

Rotarod Test

Mice were placed on a rod which is rotating at 4 rpm with an acceleration to 40 rpm within 6 min. The duration of the mice staying on the rod is measured three times at 10 min intervals and the average 'latency to fall' was determined for each mouse.

Open Field Test (OFT)

Mice were placed in a chamber measured 40 cm (length) x 40 cm (width) x 30 cm (height) and recorded for 15 min. Recorded videos were analyzed with TopScan video tracking software. The mice path tracking and time spent in the defined area were analyzed. The mice used for two age groups: 2-3 months old (n= 7) and 6-8 months old (n= 6), unless otherwise stated.

For drug treatment open field test, after 15 min baseline recording, intraperitoneal injections of amphetamine at 3.0 mg/kg (D961, Age D'or) or SKF81297 at 2.5mg/kg (S143, Sigma-Aldrich) or quinpirole at 0.2mg/kg (sc-253339, Santa Cruz) were administered, dosage was optimized with reference to literature(Delignat-Lavaud *et al.*, 2023). Total traveled distance of the mice after 60 min injection was recorded by the tracking system and the results were normalized to individual baseline. Traveled distance was expressed by percent of baseline. Percent of baseline was calculated per animal as (post_mean / baseline_mean) × 100, where baseline_mean is the mean distance over the 15-min pre-drug period and post_mean is the mean distance over the 60 min post-drug test.

Quantification of DAT Immunoreactivity Clusters and TH+ Striatal Interneurons

The quantification of DAT-positive clustering in striatum was conducted using Fiji software (Version ImageJ 2.160/1.54p/Java 1.8.0_322 (64-bit), RRID: SCR_002285). For each mouse, 5 random sampling sites with a size of 300 µm x 300 µm were selected respectively for both dorsal and ventral striatum. At least three mice from each genotype and each age group were collected for this purpose. The threshold setting for the clusters was set to quantify puncta bigger than 5 μm^2 to ensure normal positive axonal terminals were not counted in. The average size of clusters and average number of clusters was counted automatically with Fiji plugin “Analyse Particles” based on all five random sampling sites for each mouse. Density of clusters was calculated as the number of clusters per ROI area and normalized to a standard 300 × 300 μm^2 area.

Quantification of TH-positive and tdT-expressing cells was done using Fiji software with full stitched half coronal section. Image acquisition involved tiling of the entire section with either 10x or 20x objective lens on Andor BC43. Cell Counter plugin in Fiji software was used to count visible cell bodies across the striatum (outlined based on Allen mouse brain atlas). Cell count from individual channels was used for percentage ratio quantification.

Quantification for TH-positive cells intensity was done using Fiji software. A consistent threshold was applied across all images to isolate TH-positive signals. The 8-bit figure type was used to measure the mean density of the TH signal. Background fluorescence was determined from adjacent areas without specific staining. All measurements were performed under identical settings to ensure consistency across experimental groups. For each mouse, 6 random TH-positive cells were selected from both dorsal and ventral striatum. At least three mice from each condition were collected for this purpose.

Statistical Analysis

All statistical analysis was performed using GraphPad Prism (Ver 10.4.1, RRID: SCR_002798). All graphs were plotted on GraphPad Prism. Data are presented as mean ± SEM unless otherwise stated. Comparisons between two independent groups were conducted using Welch’s unpaired t-test. For analyses involving more than two groups, one-way or two-way ANOVA with Tukey’s honestly significant difference (HSD) post hoc test was applied. For repeated measures data from the 60 min open field test, two-way ANOVA with Tukey’s HSD post hoc test was performed. Data with *p*-values <0.05, <0.01, <0.001, and <0.0001 are represented by asterisks *, **, ***, and ****.

References

Anderegg A, Poulin J-F, Awatramani R (2015) Molecular heterogeneity of midbrain dopaminergic neurons – Moving toward single cell resolution. *FEBS Letters* 589: 3714-3726

Bandres-Ciga S, Diez-Fairen M, Kim JJ, Singleton AB (2020) Genetics of Parkinson's disease: An introspection of its journey towards precision medicine. *Neurobiol Dis* 137: 104782

Betarbet R, Turner R, Chockkan V, DeLong MR, Allers KA, Walters J, Levey AI, Greenamyre JT (1997) Dopaminergic neurons intrinsic to the primate striatum. *J Neurosci* 17: 6761-6768

Busceti CL, Bucci D, Molinaro G, Di Pietro P, Zangrandi L, Gradini R, Moratalla R, Battaglia G, Bruno V, Nicoletti F *et al* (2012) Lack or Inhibition of Dopaminergic Stimulation Induces a Development Increase of Striatal Tyrosine Hydroxylase-Positive Interneurons. *PloS one* 7: e44025

Cai H, Liu G, Sun L, Ding J (2014) Aldehyde Dehydrogenase 1 making molecular inroads into the differential vulnerability of nigrostriatal dopaminergic neuron subtypes in Parkinson's disease. *Translational Neurodegeneration* 3

Cai X, Liu C, Tsutsui-Kimura I, Lee J-H, Guo C, Banerjee A, Lee J, Amo R, Xie Y, Patriarchi T *et al* (2024) Dopamine dynamics are dispensable for movement but promote reward responses. *Nature* 635: 406-414

Cao M, Park D, Wu Y, De Camilli P (2020) Absence of Sac2/INPP5F enhances the phenotype of a Parkinson's disease mutation of synaptojanin 1. *Proc Natl Acad Sci U S A* 117: 12428-12434

Cao M, Wu Y, Ashrafi G, McCartney AJ, Wheeler H, Bushong EA, Boassa D, Ellisman MH, Ryan TA, De Camilli P (2017) Parkinson Sac Domain Mutation in Synaptojanin 1 Impairs Clathrin Uncoating at Synapses and Triggers Dystrophic Changes in Dopaminergic Axons. *Neuron* 93: 882-896 e885

Chanaday NL, Cousin MA, Milosevic I, Watanabe S, Morgan JR (2019) The Synaptic Vesicle Cycle Revisited: New Insights into the Modes and Mechanisms. *The Journal of Neuroscience* 39: 8209

Cossette M, Lecomte F, Parent A (2005) Morphology and distribution of dopaminergic neurons intrinsic to the human striatum. *J Chem Neuroanat* 29: 1-11

Cremona O, Di Paolo G, Wenk MR, Luthi A, Kim WT, Takei K, Daniell L, Nemoto Y, Shears SB, Flavell RA *et al* (1999) Essential role of phosphoinositide metabolism in synaptic vesicle recycling. *Cell* 99: 179-188

Darmopil S, Muñetón-Gómez VC, De Ceballos ML, Bernson M, Moratalla R (2008) Tyrosine hydroxylase cells appearing in the mouse striatum after dopamine denervation are likely to be projection neurones regulated by l -DOPA. *European Journal of Neuroscience* 27: 580-592

Delignat-Lavaud B, Kano J, Ducrot C, Masse I, Mukherjee S, Giguere N, Moquin L, Levesque C, Burke S, Denis R *et al* (2023) Synaptotagmin-1-dependent phasic axonal dopamine release is dispensable for basic motor behaviors in mice. *Nat Commun* 14: 4120

Dubach M, Schmidt R, Kunkel D, Bowden DM, Martin R, German DC (1987) Primate neostriatal neurons containing tyrosine hydroxylase: Immunohistochemical evidence. *Neuroscience Letters* 75: 205-210

Dyment DA, Smith AC, Humphreys P, Schwartzentruber J, Beaulieu CL, Consortium FC, Bulman DE, Majewski J, Woulfe J, Michaud J *et al* (2015) Homozygous nonsense mutation in SYNJ1 associated with intractable epilepsy and tau pathology. *Neurobiology of aging* 36: 1222 e1221-1225

Erben L, Welday JP, Murphy R, Buonanno A (2022) Toxic and Phenotypic Effects of AAV_Cre Used to Transduce Mesencephalic Dopaminergic Neurons. *International Journal of Molecular Sciences* doi: 10.3390/ijms23169462 [PREPRINT]

Farrow SL, Schierding W, Gokuladhas S, Golovina E, Fadason T, Cooper AA, O'Sullivan JM (2022) Establishing gene regulatory networks from Parkinson's disease risk loci. *Brain* 145: 2422-2435

Gao X, Huang Z, Feng C, Guan C, Li R, Xie H, Chen J, Li M, Que R, Deng B *et al* (2020) Multimodal analysis of gene expression from postmortem brains and blood identifies synaptic vesicle trafficking genes to be associated with Parkinson's disease. *Brief Bioinform*

Hardies K, Cai Y, Jardel C, Jansen AC, Cao M, May P, Djémié T, Hachon Le Camus C, Keymolen K, Deconinck T *et al* (2016) Loss of SYNJ1 dual phosphatase activity leads to early onset refractory seizures and progressive neurological decline. *Brain* 139: 2420-2430

Hayashi M, Raimondi A, O'Toole E, Paradise S, Collesi C, Cremona O, Ferguson SM, De Camilli P (2008) Cell- and stimulus-dependent heterogeneity of synaptic vesicle endocytic recycling mechanisms revealed by studies of dynamin 1-null neurons. *Proc Natl Acad Sci U S A* 105: 2175-2180

Huot P, Levesque M, Parent A (2006) The fate of striatal dopaminergic neurons in Parkinson's disease and Huntington's chorea. *Brain* 130: 222-232

Ibáñez-Sandoval O, Tecuapetla F, Unal B, Shah F, Koós T, Tepper JM (2010) Electrophysiological and Morphological Characteristics and Synaptic Connectivity of Tyrosine Hydroxylase-Expressing Neurons in Adult Mouse Striatum. *The Journal of Neuroscience* 30: 6999-7016

Krebs CE, Karkheiran S, Powell JC, Cao M, Makarov V, Darvish H, Di Paolo G, Walker RH, Shahidi GA, Buxbaum JD *et al* (2013) The Sac1 domain of SYNJ1 identified mutated in a family with early-onset progressive Parkinsonism with generalized seizures. *Hum Mutat* 34: 1200-1207

Lesage S, Mangone G, Tesson C, Bertrand H, Benmahdjoub M, Kesraoui S, Arezki M, Singleton A, Corvol JC, Brice A (2021) Clinical Variability of SYNJ1-Associated Early-Onset Parkinsonism. *Front Neurol* 12: 648457

Mao M, Nair A, Augustine GJ (2019) A Novel Type of Neuron Within the Dorsal Striatum. *Frontiers in Neural Circuits* 13: 32

Masuda M, Miura M, Inoue R, Imanishi M, Saino-Saito S, Takada M, Kobayashi K, Aosaki T (2011) Postnatal development of tyrosine hydroxylase mRNA-expressing neurons in mouse neostriatum. *European Journal of Neuroscience* 34: 1355-1367

Mejaes JI, Saenz J, O'Brien C, Pizzano CM, Pan PY, Barker DJ (2024) Haploinsufficiency of the Parkinson's disease gene synaptojanin1 is associated with abnormal responses to psychomotor stimulants and mesolimbic dopamine signaling. *Front Behav Neurosci* 18: 1359225

Milosevic I, Giovedi S, Lou X, Raimondi A, Collesi C, Shen H, Paradise S, O'Toole E, Ferguson S, Cremona O *et al* (2011) Recruitment of Endophilin to Clathrin-Coated Pit Necks Is Required for Efficient Vesicle Uncoating after Fission. *Neuron* 72: 587-601

Nakahara T, Yamamoto T, Endo K, Kayama H (2001) Neuronal ectopic expression of tyrosine hydroxylase in the mouse striatum by combined administration of 1-methyl-4-phenyl-1,2,3,6-tetrahydropyridine and 3-nitropropionic acid. *Neuroscience* 108: 601-610

Nalls MA, Pankratz N, Lill CM, Do CB, Hernandez DG, Saad M, DeStefano AL, Kara E, Bras J, Sharma M *et al* (2014) Large-scale meta-analysis of genome-wide association data identifies six new risk loci for Parkinson's disease. *Nature Genetics* 46: 989-993

Ng XY, Cao M (2024) Dysfunction of synaptic endocytic trafficking in Parkinson's disease. *Neural Regen Res* 19: 2649-2660

Ng XY, Wu Y, Lin Y, Yaqoob SM, Greene LE, De Camilli P, Cao M, (2023) Mutations in Parkinsonism-linked endocytic proteins synaptojanin1 and auxilin have synergistic effects on dopaminergic axonal pathology. *npj Parkinson's Disease* 9

Özçete ÖD, Banerjee A, Kaeser PS (2024) Mechanisms of neuromodulatory volume transmission. *Molecular Psychiatry* 29: 3680-3693

Palfi S, Leventhal L, Chu Y, Ma SY, Emborg M, Bakay R, Déglon N, Hantraye P, Aebischer P, Kordower JH (2002) Lentivirally Delivered Glial Cell Line-Derived Neurotrophic Factor Increases the Number of Striatal Dopaminergic Neurons in Primate Models of Nigrostriatal Degeneration. *The Journal of Neuroscience* 22: 4942

Pan P-Y, Zhu J, Rizvi A, Zhu X, Tanaka H, Dreyfus CF (2021) Synaptojanin1 deficiency upregulates basal autophagosome formation in astrocytes. *Journal of Biological Chemistry* 297

Pan PY, Li X, Wang J, Powell J, Wang Q, Zhang Y, Chen Z, Wicinski B, Hof P, Ryan TA *et al* (2017) Parkinson's Disease-Associated LRRK2 Hyperactive Kinase Mutant Disrupts Synaptic Vesicle Trafficking in Ventral Midbrain Neurons. *J Neurosci* 37: 11366-11376

Pan PY, Sheehan P, Wang Q, Zhu X, Zhang Y, Choi I, Li X, Saenz J, Zhu J, Wang J *et al* (2020) Synj1 haploinsufficiency causes dopamine neuron vulnerability and alpha-synuclein accumulation in mice. *Hum Mol Genet* 29: 2300-2312

Porritt MJ, Batchelor PE, Hughes AJ, Kalnins R, Donnan GA, Howells DW (2000) New dopaminergic neurons in Parkinson's disease striatum. *Lancet* 356: 44-45

Quadri M, Fang M, Picillo M, Olgiati S, Breedveld GJ, Graafland J, Wu B, Xu F, Erro R, Amboni M *et al* (2013) Mutation in the SYNJ1 gene associated with autosomal recessive, early-onset Parkinsonism. *Hum Mutat* 34: 1208-1215

Ramírez-Jarquín UN, Sharma M, Shahani N, Li Y, Boregowda S, Subramaniam S (2022) Rhes protein transits from neuron to neuron and facilitates mutant huntingtin spreading in the brain. *Science Advances* 8: eabm3877

Rauschendorf MA, Jost M, Stock F, Zimmer A, Rosler B, Rijntjes M, Piroth T, Coenen VA, Reinacher PC, Meyer PT *et al* (2017) Novel compound heterozygous synaptojanin-1 mutation causes l-dopa-responsive dystonia-parkinsonism syndrome. *Mov Disord* 32: 478-480

Rezai Amin S, Gruszczynski C, Guiard BP, Callebert J, Launay J-M, Louis F, Betancur C, Vialou V, Gautron S (2019) Viral vector-mediated Cre recombinase expression in substantia nigra induces lesions of the nigrostriatal pathway associated with perturbations of dopamine-related behaviors and hallmarks of programmed cell death. *Journal of Neurochemistry* 150: 330-340

Rice ME, Patel JC, Cragg SJ (2011) Dopamine release in the basal ganglia. *Neuroscience* 198: 112-137

Rufino-Ramos D, Leandro K, Perdigão PRL, O'Brien K, Pinto MM, Santana MM, van Solinge TS, Mahjoum S, Breakefield XO, Breyne K *et al* (2023) Extracellular communication between brain cells through functional transfer of Cre mRNA mediated by extracellular vesicles. *Molecular Therapy* 31: 2220-2239

Saheki Y, De Camilli P (2012) Synaptic vesicle endocytosis. *Cold Spring Harbor perspectives in biology* 4: a005645

Schuske KR, Richmond JE, Matthies DS, Davis WS, Runz S, Rube DA, van der Bliek AM, Jorgensen EM (2003) Endophilin Is Required for Synaptic Vesicle Endocytosis by Localizing Synaptojanin. *Neuron* 40: 749-762

Senkevich K, Parlar SC, Chantereault C, Yu E, Ahmad J, Ruskey JA, Asayesh F, Spiegelman D, Waters C, Monchi O *et al* (2024) Are rare heterozygous SYNJ1 variants associated with Parkinson's disease? *NPJ Parkinsons Dis* 10: 201

Tande D, Hoglinger G, Debeir T, Freundlieb N, Hirsch EC, Francois C (2006) New striatal dopamine neurons in MPTP-treated macaques result from a phenotypic shift and not neurogenesis. *Brain* 129: 1194-1200

Tashiro Y, Sugimoto T, Hattori T, Uemura Y, Nagatsu I, Kikuchi H, Mizuno N (1989) Tyrosine hydroxylase-like immunoreactive neurons in the striatum of the rat. *Neuroscience Letters* 97: 6-10

Tepper JM, Koós T, Ibanez-Sandoval O, Tecuapetla F, Faust TW, Assous M (2018) Heterogeneity and Diversity of Striatal GABAergic Interneurons: Update 2018. *Frontiers in Neuroanatomy* 12: 91

Troshev D, Bannikova A, Blokhin V, Kolacheva A, Pronina T, Ugrumov M (2022) Striatal Neurons Partially Expressing a Dopaminergic Phenotype: Functional Significance and Regulation. *International Journal of Molecular Sciences* 23: 11054

Troshev D, Bannikova A, Blokhin V, Pavlova E, Kolacheva A, Ugrumov M (2023) Compensatory Processes in Striatal Neurons Expressing the Tyrosine Hydroxylase Gene in Transgenic Mice in a Model of Parkinson’s Disease. *International Journal of Molecular Sciences* 24: 16245

Ünal B, Shah F, Kothari J, Tepper JM (2015) Anatomical and electrophysiological changes in striatal TH interneurons after loss of the nigrostriatal dopaminergic pathway. *Brain Structure and Function* 220: 331-349

Verstreken P, Koh T-W, Schulze KL, Zhai RG, Hiesinger PR, Zhou Y, Mehta SQ, Cao Y, Roos J, Bellen HJ (2003) Synaptojanin Is Recruited by Endophilin to Promote Synaptic Vesicle Uncoating. *Neuron* 40: 733-748

Xenias HS, Ibáñez-Sandoval O, Koós T, Tepper JM (2015) Are Striatal Tyrosine Hydroxylase Interneurons Dopaminergic? *The Journal of Neuroscience* 35: 6584-6599

Zhu X, Prakash SS, McAuliffe G, Pan P-Y (2023) Synaptojanin1 Modifies Endolysosomal Parameters in Cultured Ventral Midbrain Neurons. *eneuro* 10

Acknowledgment

We thank Prof Zhang Suchun (Duke-NUS) and Asst Prof Jun Nishiyama (Duke-NUS) for providing some reagents for the experiments. We thank Prof Pietro De Camili (Yale University), Prof Shirish Shenolikar (Duke University) and Prof Wang Hongyan (Duke-NUS) for reading the manuscript and providing comments. We thank Dr Sarah Luo Xinwei (IMCB-A*STAR) and Prof Enrico Petretto (Duke-NUS) for kindly providing TH-IRES-Cre mouse line and Ai9 mouse line, respectively. We also thank Prof Pietro De Camili for gifting SJ1-KI^{RQ} mouse line. We thank Asst Prof Wong Peiyan (Duke-NUS) from animal behaviour core for training. We thank Electron Microscopy Unit (NUS) for EM preparation and imaging. Some illustrations were created using BioRender. Select portions of this manuscript were edited for clarity and grammar using the ChatGPT language model (OpenAI). Scientific content and interpretations were solely formulated by the authors. This research was supported in part by grant from Ministry of Education Academic Research Fund (AcRF) Singapore Tier 2 (MOE-T2EP30122-0009) and Tier 1 (FY2024-MOET1-0001).

Declaration of interest

The authors declare no competing interests.

Data and materials availability

The datasets generated and/or analyzed in this study are available from the corresponding author Mian Cao on request. All other data needed to evaluate the conclusions in the paper are present in the paper and/or the Supplementary Materials.

Author Contributions

Y.L., B.M., M.L., Z.L. and M.C. designed the experiments. Y.L., M.L. and Z.L. performed sample preparations, histology experiments and microscopy imaging. Y.L. and X.C performed HPLC and analysis. Y.L. performed western blotting and analysis. Y.L. and M.C. performed sample preparations for EM. Y.L., B.M., M.L., X.C. and Z.W. performed behavioural experiments. B.M., M.L. and Z.L. performed stereotaxic injections. Y.L. and M.L. performed quantifications and statistical analysis for clusters and behavioural assays. M.L. and X.C. performed mice genotyping. Y.L., B.M. and M.C. wrote the paper. M.L. and Z.L.

reviewed the text and contributed to its revision. All authors read and approved the final manuscript.

Supplemental information

Document S1. Figures S1–S11 and Table S1

Figure Legends

Figure 1. SJ1 conditional KO (SJ1 cKO^{DAT}) in DA neurons exhibit dystrophic DA axon terminals in the striatum

(A) Generation of SJ1 cKO^{DAT} mice by crossing SJ1 flx/flx mice with DAT-IRES-Cre line to create DA-specific SJ1 conditional KO mice (DAT-Cre;SJ1 flx/flx), hereafter referred to as SJ1 cKO^{DAT}. Appropriate littermate control (SJ1 flx/flx or DAT-Cre;SJ1+/flx) were used in all experiments.

(B) Double staining of TH and SJ1 to show SJ1 specifically KO in midbrain DA neurons. Green arrows: TH-positive DA neurons; White arrows: TH-negative midbrain neurons. SJ1 expression in hippocampus shows that other regions were not affected. Scale bar: 20 μm.

(C) DAT staining of 2 months old Ctrl and SJ1 cKO^{DAT} shows clustering phenotype in dorsal (DS) and ventral striatum (VS). Scale bar: 20 μm.

(D) Quantification for DAT clusters at 2-3 months and 6-8 months of age. The average number of clusters is counted in five randomly selected, 300 × 300-μm regions of interest (ROIs). Data are represented as mean ± SEM (*p<0.01 and ***p<0.001 by one-way ANOVA with post-hoc Tukey's test). n=3 mice per genotype.

(E) Double staining of DAT with TH, AADC, vMAT2 and SV2C showed colocalization in the dorsal striatum (DS) of SJ1 cKO^{DAT} mice. Scale bar: 20 μm.

(F) Representative EM micrographs of nerve terminals from the ventral striatum (VS) of SJ1 cKO^{DAT}. Red arrows: "Whirl"-like multilayered membranes; Synaptic vesicles (SVs), endosomes (endo), autophagosome (AP) and mitochondria (mt) were also labeled in the images. Scale bar: 500 nm.

Figure 2. Dysregulated DA system and impaired DA release in SJ1 cKO^{DAT} striatum

(A), (B) Representative western blot and analysis for DA markers, endocytic and general synaptic markers from 2-3 months old Ctrl and SJ1 cKO^{DAT} half brain striatal homogenates. DAT and vMAT2 in SJ1 cKO^{DAT} exhibited significant reduction after normalization. Data are represented as mean ± SEM (*p<0.05 and **p<0.01 with Welch's unpaired t-test). n=3-5 mice per genotype.

(C), (D) HPLC analysis of SJ1 cKO^{DAT} mice showed an average of 50% reduction in striatal DA level, enhanced HVA level and non-significant change in DOPAC level for 2-3 months old

(C) and 6-8 months old (D). Data are represented as mean ± SEM (*p<0.05 and **p<0.01 with Welch's unpaired t-test). n number used for each genotype=5 for 2-3M; n=6 for 6-8M.

(E) Illustration of KCl-evoked DA release in DA terminals.

(F) Illustration of AMPH-induced DA efflux in DA terminals.

(G) Quantification of normalized DA concentration from KCl-evoke DA release in SJ1 cKO^{DAT} acute striatal slices revealed significant reduction, suggesting impaired vesicular release. Data are represented as mean ± SEM (*p<0.05 with Welch's unpaired t-test). n=3 mice per genotype.

(H) Quantification of normalized DA concentration from AMPH-induced DA efflux in SJ1 cKO^{DAT} acute striatal slices revealed significant reduction, suggesting reduced DAT-mediated DA efflux. Data are represented as mean ± SEM (**p<0.01 with Welch's unpaired t-test). n=3 mice per genotype.

Figure 3. SJ1 cKO^{DAT} displayed altered locomotor activity but no coordination deficit

(A) Representative open-field activity traces (15 min) from Ctrl and SJ1 cKO^{DAT} mice at both time points illustrate reduced locomotor activity observed in mutants.

(B) Total distance traveled in open field test was recorded for 15 min. Significant p-value for total distance at both 2-4 and 6-8 months old SJ1 cKO^{DAT} mice indicate reduced spontaneous locomotion during baseline. Data are represented as mean ± SEM (*p<0.05 and **p<0.01 with Welch's unpaired t-test). n numbers used for each age group (2-4M: 7; 6-8M: 6).

(C), (D) Quantification of average distance traveled, expressed as percent of baseline, over the time course. Locomotor activity (% of baseline) of SJ1 cKO^{DAT} mice increased over 60 min session treated with 3mg/kg amphetamine (AMPH). Data are represented as mean ± SEM (*p<0.05 and **p<0.01 by two-way repeated measures ANOVA with post-hoc Tukey's test). n numbers used for each age group (2-4M: 7; 6-8M: 6).

(E) Representative open-field activity traces (60 min) from Ctrl and SJ1 cKO^{DAT} mice at both time points illustrate AMPH-induced heightened hyperactivity observed in mutants.

(F), (G) Average traveled distance in the open field. % of baseline across 60 min session in 2-4 (F) and 6-8 (G) months old treated with 3 mg/kg AMPH show significant increase in mutant's locomotion. Data are represented as mean ± SEM (*p<0.05, **p<0.01 by Welch's t test). n numbers used for each age group (2-4M: 7; 6-8M: 6).

(H),(I) Average total distance traveled over the time course (H) and average distance traveled in open field (I), both expressed as percent of baseline, showing significantly elevated locomotion in SJ1 cKO^{DAT} mice (age range 4-10M) in response to D1R agonist, SKF81297 at 2.5mg/kg. Data are represented as mean ± SEM (*p<0.05 and **p<0.01 by two-way repeated measures ANOVA with post-hoc Tukey's test). n=6 per genotype.

(J),(K) Average total distance traveled over the time course (H) and average distance traveled in open field (I), both expressed as percent of baseline, showing comparable reduced locomotion in Ctrl and SJ1 cKO^{DAT} mice (age range 6-8M) in response to D2R agonist, quinpirole at 0.2mg/kg. Data are represented as mean ± SEM. n=6 per genotype.

(L) Accelerated rotarod performance of two age groups. Latency to fall did not differ significantly between Ctrl and SJ1 cKO^{DAT} mice. Data are represented as mean ± SEM. n numbers used for Ctrl and SJ1 cKO^{DAT} mice (2–3M: 13 and 15; 6–8 M: 9 and 10).

(M) Number of missteps during the balance beam test did not differ significantly between Ctrl and SJ1 cKO^{DAT} mice. Data are represented as mean ± SEM. n numbers used for Ctrl and SJ1 cKO^{DAT} mice (2–3M: 13 and 15; 6–8M: 9 and 10).

Figure 4. Robust appearance of induced TH-positive interneurons (iTHINs) with DA-like characteristics in the SJ1 cKO^{DAT} striatum

(A) Robust emergence of iTHINs observed in the striatum of 2 months old SJ1 cKO^{DAT} mice but not in Ctrl. Scale bar: 50 µm.

(B) Quantification of iTHINs in 2-3 months and 6-8 months shows significant higher number in SJ1 cKO^{DAT} striatum. Number of iTHINs were quantified on single coronal striatum section of one hemisphere. Data are represented as mean ± SEM (**p<0.01). n=3 mice per genotype.

(C) Representative image of iTHINs expressing AADC in the striatum of 2 months old SJ1 cKO^{DAT} mice compared to Ctrl. White arrows: iTHINs. Asterisk: clusters. Scale bar: 20 µm.

(D) Double staining of vMAT2 and TH shows vMAT2 is clustered with TH at DA terminals but not expressed in iTHINs in 2 months old SJ1 cKO^{DAT} striatum. White arrows: iTHINs. Asterisk: clusters. Scale bar: 20 µm.

(E) Double staining of DAT and TH shows DAT is clustered with TH at DA terminals but not expressed in iTHINs in 2 months old SJ1 cKO^{DAT} striatum. White arrows: iTHINs. Asterisk: clusters. Scale bar: 20 µm.

(F), (G) Double staining of ALDH1A1 and TH shows ALDH1A1 is detected in both dystrophic DA terminals and iTHINs in SJ1 cKO^{DAT} dorsal (F) but not ventral (G) striatum. White arrows: iTHINs. Asterisk: clusters. Scale bar: 50 µm.

Figure 5. SJ1 conditional KO using TH-IRES-Cre (SJ1 cKOTH) phenocopies SJ1 cKO^{DAT} pathological characteristics

(A) Generation of SJ1 cKOTH mice by crossing SJ1 flx/flx mice with TH-IRES-Cre line to create TH-specific SJ1 conditional KO mice (TH-Cre;SJ1 flx/flx), hereafter referred to as SJ1 cKOTH. Appropriate littermate controls (SJ1 flx/flx or TH-Cre;SJ1 +/flx) were used in all experiments.

(B) Double staining of TH and SJ1 showed specific loss of SJ1 in DA neurons. SJ1 expression in hippocampus shows that other regions were not affected. Scale bar: 20 µm.

(C) DAT staining of 2 months old Ctrl and SJ1 cKOTH showed similar clustering phenotype in dorsal and ventral striatum. Scale bar: 20 µm.

(D) Double staining of vMAT2 with SV2C showed co-aggregation in the striatum of SJ1 cKOTH mice. Scale bar: 20 µm.

(E) Double staining of DAT and TH showed DAT is clustered with TH at DA terminals (asterisk) but not expressed in iTHINs (white arrows) in the striatum of SJ1 cKOTH mice. Scale bar: 20 µm.

(F) Double staining of AADC and TH showed AADC is clustered with TH at DA terminals (asterisk) and co-expressed in iTHINs (white arrows). Scale bar: 20 µm.

(G), (H) Double staining of ALDH1A1 and TH shows ALDH1A1 is detected in both dystrophic DA terminals (asterik) and iTHINs (white arrows) in SJ1 cKO^{DAT} dorsal (G) but not ventral (H) striatum. Scale bar: 50 µm.

Figure 6. iTHINs emerge from original WT THINs and induce DAT gene expression after SJ1 loss

(A) Simplified schematic showing the generation of Ai9-tdT labeled SJ1 cKOTH and SJ1 cKO^{DAT} mice, referred to as Ai9;SJ1 cKOTH and Ai9;SJ1 cKO^{DAT}, respectively. Ai9-tdT reporter driven by CAG promoter expresses DA-specific tdT signal after Cre-mediated recombination by either TH- or DAT-IRES-Cre line.

(B) Representative images of tdT expression and immunostaining of TH in the midbrain DA neurons of 2 months old Ai9;TH-Cre (Ctrl) and Ai9;SJ1 cKOTH. Scale bar: 100 µm.

(C) Representative images of tdT expression and immunostaining of TH in the striatum of 2 months old Ai9;TH-Cre (Ctrl) and Ai9;SJ1 cKOTH. Blue arrows: tdT expressing THINs driven by TH-Cre recombination (negative for TH immunostaining). White arrows: iTHINs expressing tdT signal (positive for TH immunostaining). Scale bar: 50 µm

(D) Percentage of TH-Cre driven tdT expressing neurons positive for TH immunostaining shown in (C). In average, 34.11% of total tdT expressing neurons were positive for TH immunostaining (iTHINs). The number of neurons was quantified on a single stitched coronal striatum section for both tdT expressing neurons and tdT/TH-positive neurons. Data are represented as mean ± SEM. n=3 mice per genotype.

(E) Representative images of tdT expression and TH immunostaining of DA neurons in the midbrain of 2 months old Ai9;DAT-Cre (Ctrl) and Ai9;SJ1cKO^{DAT}. Scale bar: 100 µm.

(F) Representative images of tdT expression and immunostaining of TH and DAT in the striatum of Ai9;DAT-Cre (Ctrl) and Ai9;SJ1cKO^{DAT}. tdT expressing striatal neurons were positive for TH but not DAT immunostaining, indicating DAT gene is activated in iTHINs but DAT protein is undetected. White arrows: all tdT-expressing THINs driven by DAT-Cre that were positive for TH immunostaining. Scale bar: 50 µm.

(G) Percentage of DAT-Cre driven tdT expressing neurons positive for TH immunostaining shown in (F). Majority of tdT expressing neurons were iTHINs. The number of neurons was quantified on a single stitched coronal striatum section for both tdT expressing neurons and tdT/TH-positive neurons. Data are represented as mean ± SEM. n=3 mice per genotype.

Figure 7. iTHINs establish specific and new connection with dystrophic DA fibers in SJ1 DA cKO striatum

(A) Schematic showing experiment procedure and timeline. pAAV-FLEX-tdTomato (Cre-dependent) was injected unilaterally into the ventral midbrain of SJ1 cKOTH, SJ1 cKO^{DAT} mice and Cre mouse controls at 2-3 months old. The animal brains were collected 2 weeks post injection for IHC.

(B) Representative images of TH immunostaining and tdT expression in the injected midbrain DA neurons of both SJ1 cKOTH and SJ1 cKO^{DAT} mice. Scale bar: 100 µm.

(C) Representative images of TH immunostaining in the striatum. While tdT injection in TH-Cre and DAT-Cre mice only labeled some DA fibers, tdT injection in SJ1 cKOTH and SJ1 cKO^{DAT} labeled both DA fibers and several iTHINs. White arrows: iTHINs double positive for tdT signal and TH immunostaining. Scale bar: 50 µm.

(D Percentage of tdT expressing neurons positive for anti-TH staining in both SJ1 cKOTH and SJ1 cKO^{DAT}. The number of neurons was quantified on a single stitched coronal striatal section for both tdT and TH/tdT-positive neurons. Data are represented as mean ± SEM. n=3 mice per genotype.

(E) Schematic showing experiment procedure and timeline. rAAV-mTH-EGFP was unilaterally injected into the midbrain of B6, SJ1 cKOTH and SJ1 cKO^{DAT} mice at 2-3 months old. The animal brains were collected 2 weeks post injection for IHC.

(F) Representative images of TH immunostaining with EGFP expression in the injected midbrain DA neurons of both SJ1 cKOTH and SJ1 cKO^{DAT} mice. Scale bar: 100 µm.

(G) Representative images of TH immunostaining and EGFP expression in the striatum. No EGFP expressing THINs observed in B6 striatum. Striatum of injected SJ1 cKOTH and SJ1 cKO^{DAT} mice show EGFP specifically expressed in iTHINs. White arrows: iTHINs double positive for EGFP and anti-TH staining. Scale bar: 50 µm.

(H) Percentage of EGFP expressing neurons positive for anti-TH staining in both SJ1 cKOTH and SJ1 cKO^{DAT}. The number of neurons was quantified on a single stitched coronal striatal section for both EGFP neurons and TH/EGFP-positive neurons. Data are represented as mean ± SEM. n=3 mice per genotype.

(I) Schematic showing experiment procedure and timeline. pAAV-hSyn-mCherry was injected unilaterally in the midbrain of B6, SJ1 cKOTH and SJ1 cKO^{DAT} mice at 2-3 months old. The animal brains were collected 2 weeks post injection for IHC.

(J) Representative images of TH immunostaining and mCherry expression in the injected midbrain DA neurons of both SJ1 cKOTH and SJ1 cKO^{DAT} mice. Scale bar: 100 µm.

(K) Representative images of TH immunostaining and mCherry expression in the striatum of injected mice. No mCherry labeled THINs in B6 striatum. Striatum of injected SJ1 cKOTH and SJ1 cKO^{DAT} show mCherry specifically expressed in iTHINs. White arrows: iTHINs double positive for mCherry and anti-TH staining. Scale bar: 50 µm.

(L) Percentage of mCherry expressing neurons positive for anti-TH staining in both SJ1 cKOTH and SJ1 cKO^{DAT}. The number of neurons was quantified on a single stitched coronal

striatal section for both mCherry and TH/mCherry-positive neurons. Data are represented as mean ± SEM. n=3 mice per genotype.

Figure 8. Acute SJ1 KO in DA neurons of adult and aged mice triggers similar DA terminal pathology but fewer iTHINs

(A) Schematic showing unilateral stereotaxic injection of AAV9-TH-Cre virus into the ventral midbrain of 2 months (adult) or 12 months (aged) SJ1 flx/flx mice to obtain SJ1 acute KO in DA neurons. Animal brains were collected 3-4 months post injection for IHC.

(B) TH and SJ1 immunostaining of the adult and aged SJ1 acute KO mice showed SJ1 specific KO in the injected midbrains. Scale bar: 100 µm.

(C) DAT immunostaining of the adult and aged SJ1 acute KO mice shows similar clustering phenotype in dorsal (DS) and ventral striatum (VS) as observed in SJ1 cKO^{DAT} mice. Scale bar: 20 µm.

(D) No significant difference of the number of DAT clusters between SJ1 cKO^{DAT}, adult and aged SJ1 acute KO. The average number of clusters is counted in five randomly selected, 300 × 300-µm regions of interest (ROIs). Data are represented as mean ± SEM. n = 3-4 mice per genotype.

(E) Representative images of striatum show comparable TH/DAT-positive clusters but much lesser iTHINs in the injected hemisphere of adult and aged SJ1 acute KO mice when compared to SJ1 cKO^{DAT}. White arrows: iTHINs. Scale bar: 50 µm.

(F) Number of iTHINs in the adult and aged SJ1 acute KO is significantly lower than SJ1 cKO^{DAT} mice. Number of iTHINs was quantified in stitched coronal section of the injected striatum. Data are represented as mean ± SEM (**$p<0.01$). n=3-4 mice per genotype.

Supplementary Figure Legends

Supplementary Figure 1. Further characterization of DA system in SJ1 cKO^{DAT} mice

(A) Generation strategy to obtain SJ1 cKO^{DAT} mouse model. Heterozygous DAT-IRES-Cre line was crossed with homozygous SJ1 flx/flx to obtain double heterozygous DAT-Cre;SJ1 +/flx. Double heterozygous were further crossed with each other to obtain SJ1 cKO^{DAT} and control mice.

(B) Stereological analysis of TH-positive DA cell bodies in the SN and VTA region of Ctrl and SJ1 cKO^{DAT} mice at 2-3 months and 6-8 months age group. There is no significant loss of DA neurons in both ages. The estimated cell numbers in one hemisphere are shown. Data are represented as mean ± SEM. n=3 mice per genotype. Scale bar: 200 µm.

(C) Representative images of DAT immunostaining in the striatum of SJ1 cKO^{DAT} at 3 weeks, 2 months, 6 months and 12 months age group. Scale bar: 50 µm.

(D), (E) Tiling of a single coronal striatum section labeled for DAT in 2 months SJ1 cKO^{DAT} (D) and SJ1-KI^{RQ} mice (E). Unlike SJ1-KI^{RQ}, DAT clusters were observed in the entire striatum of SJ1 cKO^{DAT} mice, including dorsal striatum (DS) and ventral striatum (VS). Scale bar: 500 µm.

(F) Quantification for average density of DAT clusters in DS and VS shown representatively in (D). Regions of interest (ROIs) were selected from a stitched coronal section and normalized to 300 × 300-µm. Data are represented as mean ± SEM. n=3 mice per genotype.

(G) TH immunostaining in the prefrontal cortex (PFC) showing DA projections from the VTA. No obvious differences in TH-positive fibers were observed between control and mutant mice. Scale bar: 50 µm.

Supplementary Figure 2. Other markers examined in the SJ1 cKO^{DAT} striatum

(A) Immunostaining of vMAT2 with SV2C showed colocalization for clusters in the striatum of 2 months SJ1 cKO^{DAT} mice. Scale bar: 20 µm.

(B), (C) Immunostaining of DAT with Syt1 (B) and alpha-Synuclein (C) showed partial colocalization with DAT-positive clusters in the striatum of 2 months SJ1 cKO^{DAT} mice. Scale bar: 20 µm.

(D) Immunostaining of DAT with pSer129-alpha-Synuclein showed no misfolded alpha-Synuclein accumulated in DAT-positive clusters in the striatum of 2 months SJ1 cKO^{DAT} mice. Scale bar: 20 µm.

(E), (F) Immunostaining of DAT with D2R (E) and Darpp32 (F) showed no colocalization with DAT-positive clusters in the striatum of 2 months SJ1 cKO^{DAT} mice, suggesting there is no effect on postsynaptic neurons. Scale bar: 20 µm.

(G), (H) Immunostaining of DAT with GFAP (G) and Iba1 (H) showed similar glia cell pattern in both Ctrl and SJ1 cKO^{DAT} mice at 2 months old, suggesting there is no gliosis and inflammation in the striatum. Scale bar: 20 µm.

Supplementary Figure 3. Endocytic markers examined in the SJ1 cKO^{DAT} striatum

(A)-(D) Double staining of DAT with SJ1 (A), clathrin-light chain (CLC) (B), amphiphysin 1 (C) and endophilin 1 (D) showed no colocalization of these clathrin-related endocytic proteins with DAT-positive clusters in the striatum of 2 months old SJ1 cKO^{DAT} mice. Scale bar: 20 µm.

Supplementary Figure 4. More EM images of whirl-like membrane accumulation at DA terminals in SJ1 cKO^{DAT} striatum.

(A), (B) More representative EM images to show the abnormal lipid membrane accumulation which is correlated with DAT/TH-positive protein clusters in 2 months old SJ1 cKO^{DAT} striatum. Abnormal whirl-like multilayered membrane (red arrows) surrounding the synaptic vesicles (SVs) and endosomes (endo). Mitochondria (mt) also labeled in the terminals. Scale bar: 200 nm and 500nm.

Supplementary Figure 5. Distribution of iTHINs in whole striatum of SJ1 cKO^{DAT}

(A) Tiling of a single coronal striatum section with TH immunostaining in 2 months old SJ1 cKO^{DAT} mice. Insets: TH-positive clusters and iTHINs were both observed throughout the striatum, including dorsal striatum (DS), ventral striatum (VS) and olfactory tubercle (OT). Scale bar: 500 µm.

(B) Representative images of TH immunostaining in the striatum of SJ1 cKO^{DAT} at 3 weeks, 2 months, 6 months and 12 months age group. TH-positive iTHINs (white arrows) and clusters (asterisk) were labeled. Scale bar: 50 µm.

Supplementary Figure 6. iTHINs are a distinct group of striatal interneurons

(A)-(C) Immunostaining of TH with NPY (A), PV (B) and ChAT (C) in SJ1 cKO^{DAT} striatum showed that iTHINs is a distinct group of neurons from other striatal interneurons. Scale bar: 20 µm.

(D), (E) Very few iTHINs in the striatum of SJ1 cKO^{DAT} occasionally co-express Calretinin (D) and Darpp32 (E), suggesting heterogeneity within iTHINs subpopulation. Scale bar: 20 µm.

Supplementary Figure 7. A subpopulation of iTHINs in SJ1 cKO^{DAT} dorsal striatum expresses ALDH1A1

(A) Immunostaining of TH and ALDH1A1 in the midbrain of 2 months SJ1 cKO^{DAT} mice shows the ventral tier DA neurons expressing ALDH1A1. Scale bar: 20 µm.

(B) Tiling of a single coronal striatum section immunostained for TH and ALDH1A1 of 2 months old Ctrl and SJ1 cKO^{DAT} mice. TH/ALDH1A1-positive iTHINs were mainly distributed in dorsal striatum (DS). Scale bar: 500 µm

(C) Immunostaining of TH and Calbindin in the midbrain of 2 months SJ1 cKO^{DAT} mice shows some VTA DA neurons expressing Calbindin. Scale bar: 20 µm.

(D) Immunostaining shows that iTHINs in the striatum of 2 months SJ1 cKO^{DAT} mice were negative for Calbindin. Scale bar: 50 µm.

Supplementary Figure 8. Control AAV labeling for the specific DA-iTHINs connection

(A) Schematic showing experiment procedure and timeline. pAAV-FLEX-tdTomato (Cre-dependent) was injected unilaterally into the striatum of TH-Cre, DAT-Cre, SJ1 cKOTH and SJ1 cKO^{DAT} mice at 2-3 months old. Animal brains were collected for IHC 2 weeks post injection.

(B) Representative images of tdT expression and TH immunostaining in the injected striatum of SJ1 cKOTH and SJ1 cKO^{DAT} with their respective Cre line control, TH-Cre and DAT-Cre mice. In TH-Cre, tdT labeled WT THINs (red arrows) that were negative for anti-TH. In SJ1 cKOTH, TH immunostaining labeled all iTHINs (blue arrows), some tdT-expressing WT THINs (red arrow) and tdT expressing iTHINs (white arrow) were observed. No tdT-expressing neurons observed in DAT-Cre injected striatum. While TH immunostaining labeled all iTHINs

(blue arrow), tdT specifically labeled some iTHINs (white arrow) in SJ1 cKO^{DAT} mice. Scale bar: 50 µm.

(C) Schematic showing experiment procedure and timeline. rAAV-mTH-EGFP was unilaterally in the midbrain of B6, Ai9;TH-Cre and Ai9;SJ1 cKOTH mice at 2-3 months old. Animal brains were collected 2 weeks post injection for IHC.

(D) Representative images of EGFP expression, tdT expression and TH immunostaining in the striatum of injected mice. EGFP was not expressed in WT THINs (red arrows) in injected Ai9;TH-Cre mice. However, EGFP was expressed in TH/tdT-positive iTHINs (white arrows) but not TH-negative/tdT-positive WT THINs (red arrows) in Ai9;SJ1 cKOTH mice. This suggests EGFP labeling is specific to iTHINs in SJ1 cKO mice. Scale bar: 50 µm.

(E) Schematic showing experiment procedure and timeline. pAAV-hSyn-mCherry was unilaterally injected into the striatum of B6 mice at 2-3 months old. Animal brains were collected 2 weeks post injection for IHC.

(F) Representative images of mCherry expression and Darpp32 immunostaining in the striatum of injected mice. mCherry-positive neurons were randomly observed in the striatum of injected mice, with a subset of them positive for Darpp32 (white arrows). Scale bar: 50 µm.

Supplementary Figure 9. THINs appearing in 6-OHDA and Casp3 lesion mice are distinct from iTHINs observed in SJ1 cKO mice

(A) Schematic showing the midbrain of 2-3 months old B6 mice unilaterally injected with 6-OHDA and collected 2 weeks post injection for IHC.

(B) Representative coronal section shows the extent of 6-OHDA lesion in the striatum and midbrain DA neurons of B6 mice. Scale bar: 500 µm.

(C) Schematic showing the midbrain of 2-3 months old DAT-Cre mice unilaterally injected with pAAV-flex-taCasp3-TEVp (Cre-dependent) and collected 1 month post injection for IHC.

(D) Representative coronal section shows the extent of Casp3-mediated lesion in the striatum and midbrain DA neurons of DAT-Cre mice. Scale bar: 500 µm.

(E) Representative images of TH-positive neurons (white arrows) observed in the striatum of SJ1 cKO^{DAT} and lesioned hemisphere of 6-OHDA and Casp3 injected mice. Exposure time and threshold were set the same for anti-TH imaging in all three conditions. Scale bar: 20 µm.

(F) The expression level of TH protein observed in 6-OHDA and Casp3 lesioned models is significantly lower than iTHINs observed in SJ1 cKO^{DAT} striatum. Data are represented as mean ± SEM (****$p<0.0001$ by one-way ANOVA with post hoc Tukey's test). n=3 mice per genotype.

(G) Unlike iTHINs in SJ1 cKO^{DAT} mice, AADC is undetectable in either 6-OHDA or Casp3 lesioned striatum. Scale bar: 20 µm.

(H) Unlike iTHINs in SJ1 cKO^{DAT} mice, ALDH1A1 is undetectable in either 6-OHDA or Casp3 lesioned striatum. Scale bar: 20 µm.

Supplementary Figure 10. Controls for lesioned models and Summary of iTHINs

(A) Representative striatum images of Ai9;DAT-Cre mice unilaterally injected with Casp3 (Cre-mediated) in the midbrain. THINs appearing in the striatum of lesioned model (white arrows) were not expressing tdT, indicating DAT gene is not activated in lesioned model THINs. Scale bar: 200 µm.

(B) Illustration summary of the new features of THINs induced in the SJ1 DA cKO striatum.

Supplementary Figure 11. Controls for SJ1 Acute KO model

(A), (B) Representative images of adult B6 mice (2 months old) (A) and aged B6 mice (12 months old) (B) unilaterally injected with AAV-TH-Cre virus show no loss of DA neurons in the midbrain or DA fibers in the striatum, validating the safety and non-toxicity of AAV TH-Cre used. Scale bar: 200 µm.

Supplementary Table 1. Comparison of THINs observed in WT, genetic SJ1 DA cKO and acute DA lesion mouse models

Immunostaining against TH, AADC, ALDH1A1 and DAT, and Cre-dependent labeling was performed to examine the gene/protein expression of these DA markers in THINs and iTHINs.

Table S1. Immunostaining of THINs observed in genetic and lesioned mice models

Mice Model		*TH*	*AADC*	*ALDH1A1*	*DAT*
Ai9;TH-Cre	WT THINs	- (*TH gene+)	-	-	-
SJ1 cKO^{DAT}	iTHINs	+++	+++	+++ (*subregion)	- (*DAT gene+)
SJ1 cKOTH	iTHINs	+++	+++	+++ (*subregion)	-
6-OHDA model		+	-	-	-
Casp3 model		+	-	-	-

+++ positive and high expression;
+ positive and mild expression;
- negative/cannot be detected with immunostaining;
*remarks

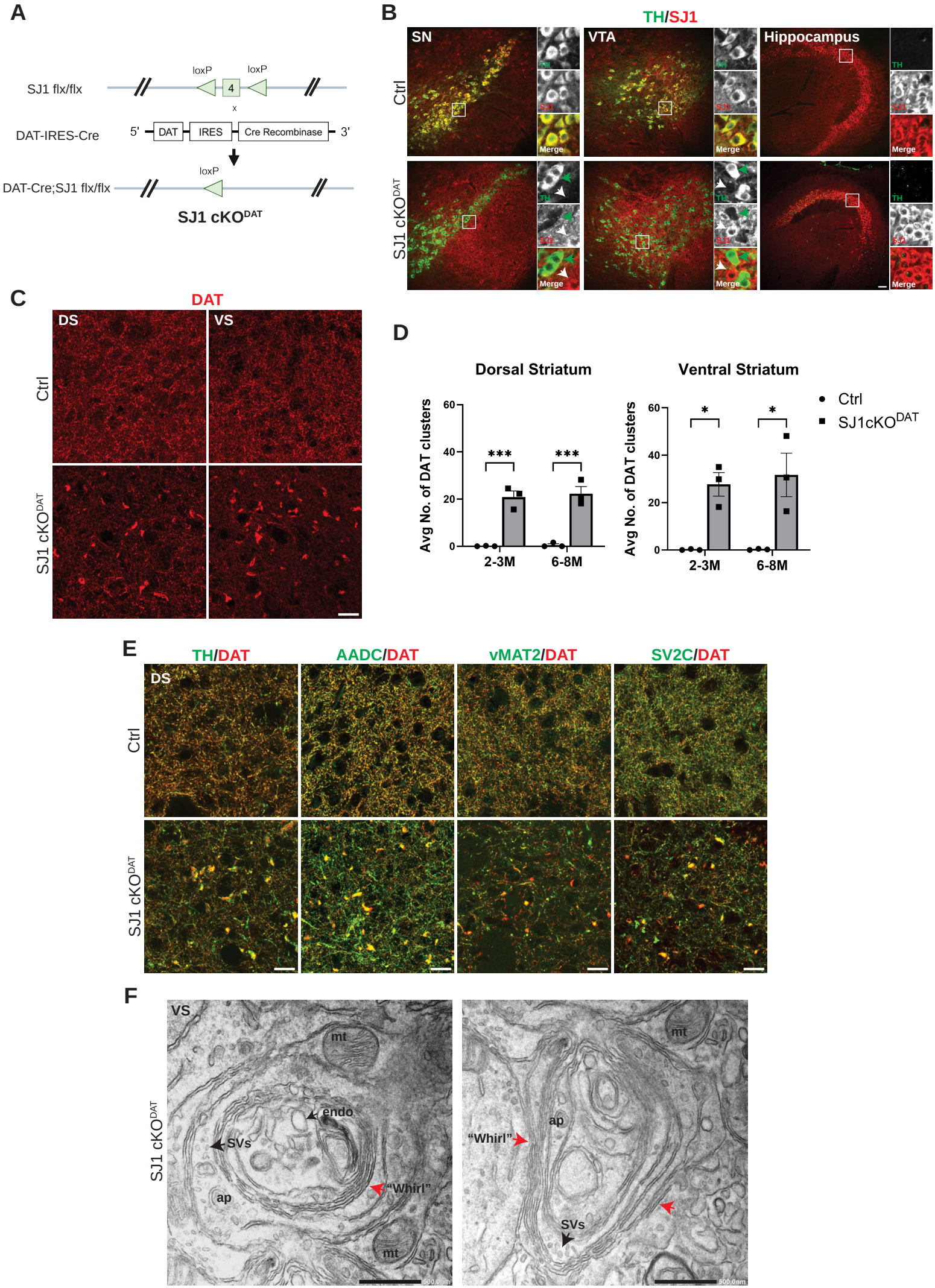
A
SJ1 flx/flx
loxP
loxP
4
x
DAT-IRES-Cre
5'
DAT
IRES
Cre Recombinase
3'
loxP
DAT-Cre;SJ1 flx/flx
SJ1 cKO^DAT
B
TH/SJ1
SN
VTA
Hippocampus
Ctrl
SJ1 cKO^DAT
TH
SJ1
Merge
C
DAT
DS
VS
Ctrl
SJ1 cKO^DAT
D
Dorsal Striatum
Ventral Striatum
Avg No. of DAT clusters
60
40
20
0
***
*
2-3M
6-8M
Ctrl
SJ1cKO^DAT
E
TH/DAT
AADC/DAT
vMAT2/DAT
SV2C/DAT
DS
Ctrl
SJ1 cKO^DAT
F
VS
mt
endo
SVs
ap
"Whirl"
SJ1 cKO^DAT
500.0nm

Figure 1

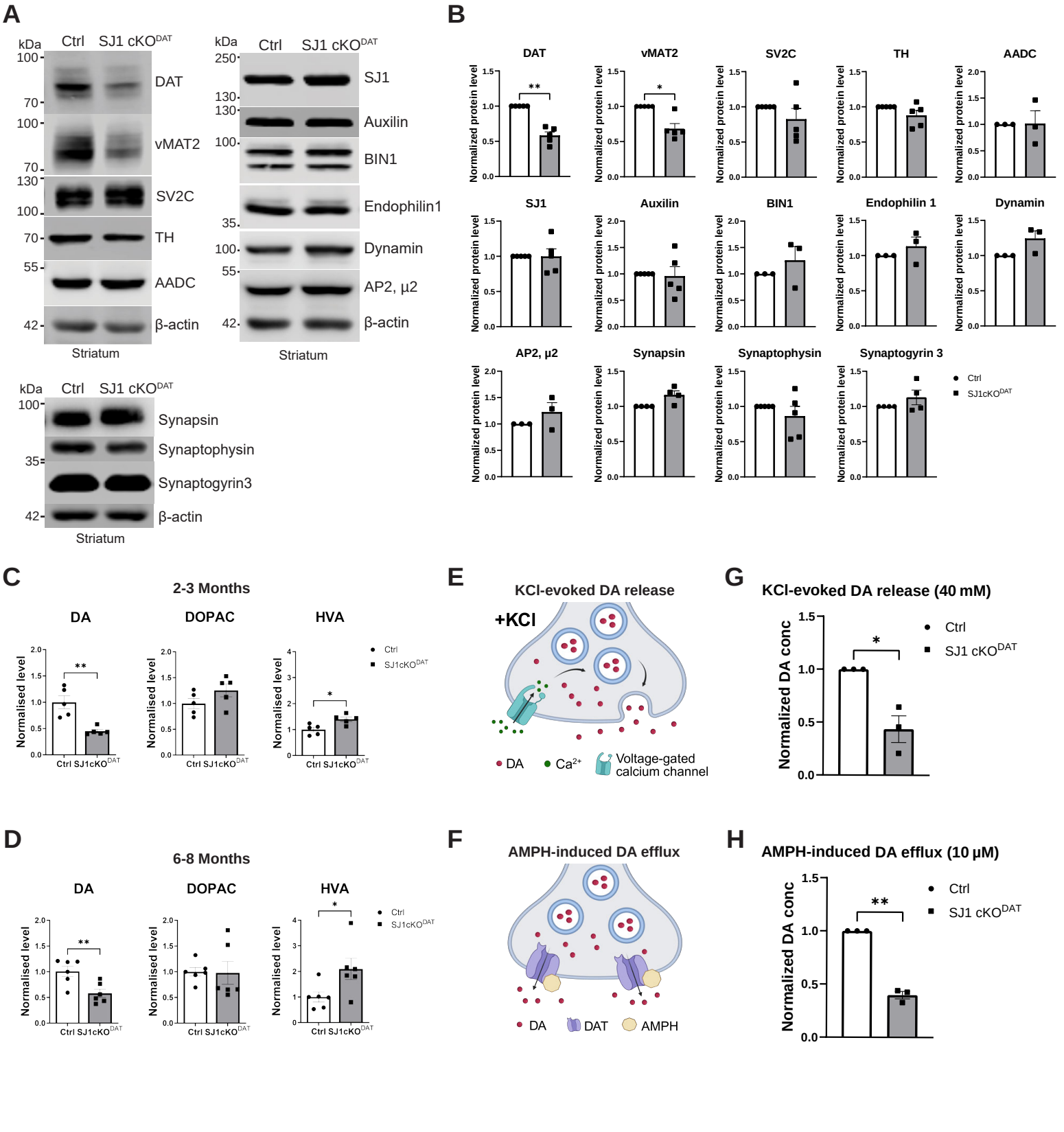
A
kDa
Ctrl
SJ1 cKO^DAT
DAT
vMAT2
SV2C
TH
AADC
β-actin
Striatum
SJ1
Auxilin
BIN1
Endophilin1
Dynamin
AP2, μ2
Synapsin
Synaptophysin
Synaptogyrin3
B
DAT
vMAT2
SV2C
TH
AADC
SJ1
Auxilin
BIN1
Endophilin 1
Dynamin
AP2, μ2
Synapsin
Synaptophysin
Synaptogyrin 3
Normalized protein level
Ctrl
SJ1cKO^DAT
C
2-3 Months
DA
DOPAC
HVA
Normalised level
D
6-8 Months
E
KCl-evoked DA release
+KCl
DA
Ca2+
Voltage-gated calcium channel
F
AMPH-induced DA efflux
DAT
AMPH
G
KCl-evoked DA release (40 mM)
Normalized DA conc
H
AMPH-induced DA efflux (10 μM)

Figure 2

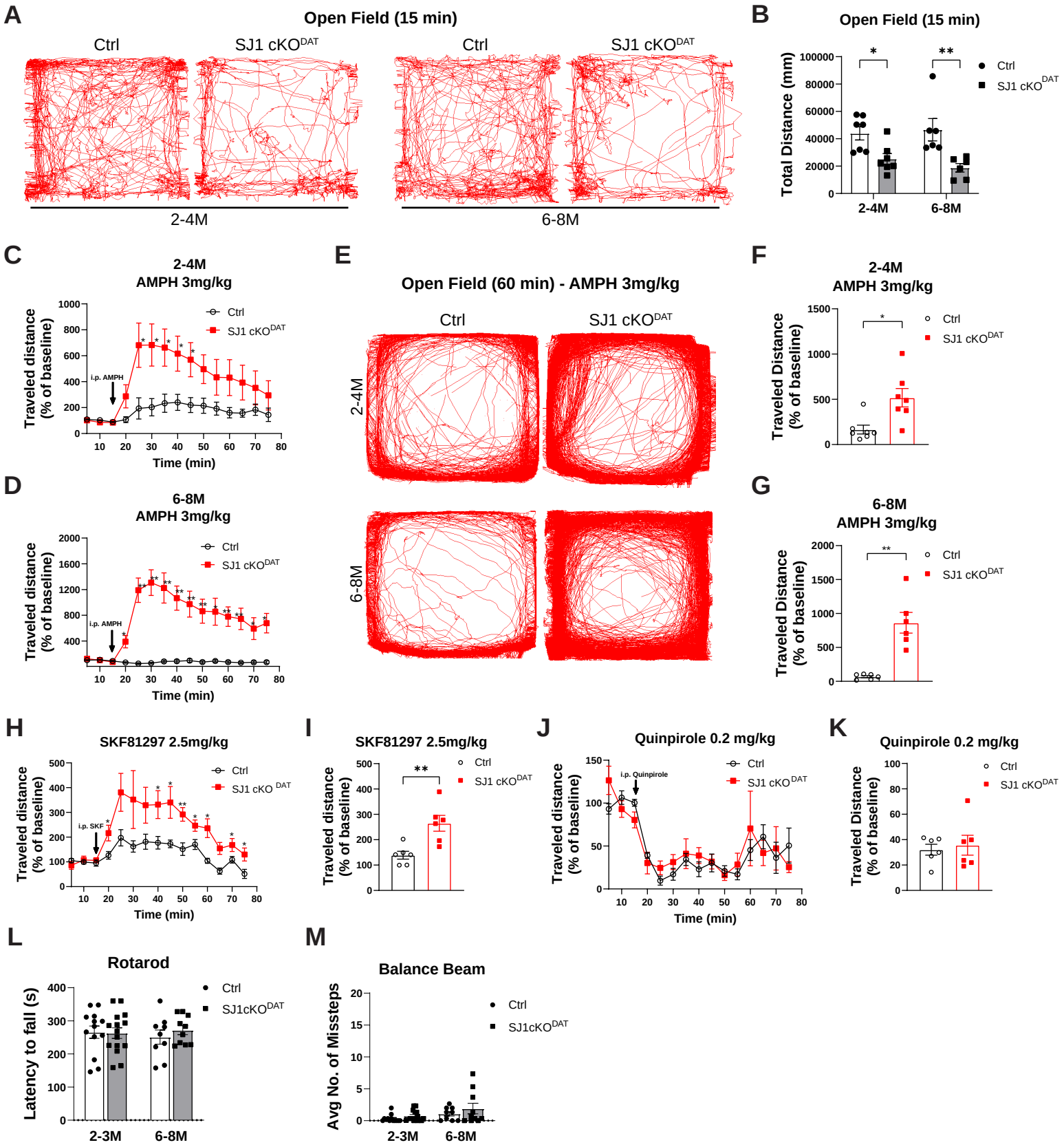
A
Open Field (15 min)
Ctrl
SJ1 cKO DAT
Ctrl
SJ1 cKO DAT
2-4M
6-8M
B
Open Field (15 min)
Total Distance (mm)
Ctrl
SJ1 cKO DAT
2-4M
6-8M
C
2-4M
AMPH 3mg/kg
Traveled distance (% of baseline)
i.p. AMPH
Time (min)
D
6-8M
AMPH 3mg/kg
E
Open Field (60 min) - AMPH 3mg/kg
F
2-4M
AMPH 3mg/kg
Traveled Distance (% of baseline)
G
6-8M
AMPH 3mg/kg
H
SKF81297 2.5mg/kg
i.p. SKF
I
SKF81297 2.5mg/kg
J
Quinpirole 0.2 mg/kg
i.p. Quinpirole
K
Quinpirole 0.2 mg/kg
L
Rotarod
Latency to fall (s)
SJ1cKO DAT
2-3M
6-8M
M
Balance Beam
Avg No. of Missteps

Figure 3

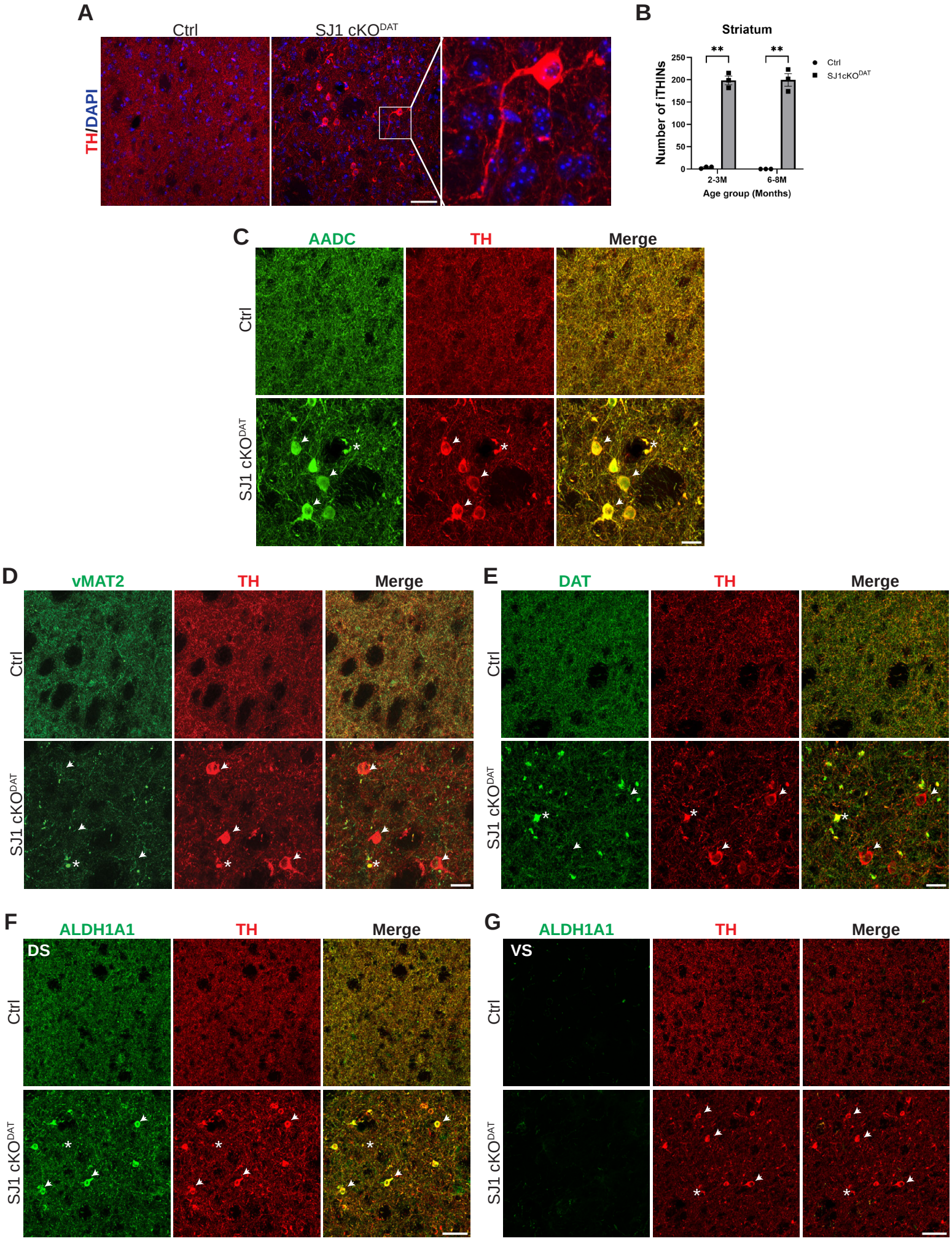
A
Ctrl
SJ1 cKO^DAT
TH/DAPI
B
Striatum
Number of iTHINs
Age group (Months)
2-3M
6-8M
Ctrl
SJ1cKO^DAT
C
AADC
TH
Merge
Ctrl
SJ1 cKO^DAT
D
vMAT2
TH
Merge
Ctrl
SJ1 cKO^DAT
E
DAT
TH
Merge
Ctrl
SJ1 cKO^DAT
F
ALDH1A1
TH
Merge
DS
Ctrl
SJ1 cKO^DAT
G
ALDH1A1
TH
Merge
VS
Ctrl
SJ1 cKO^DAT

Figure 4

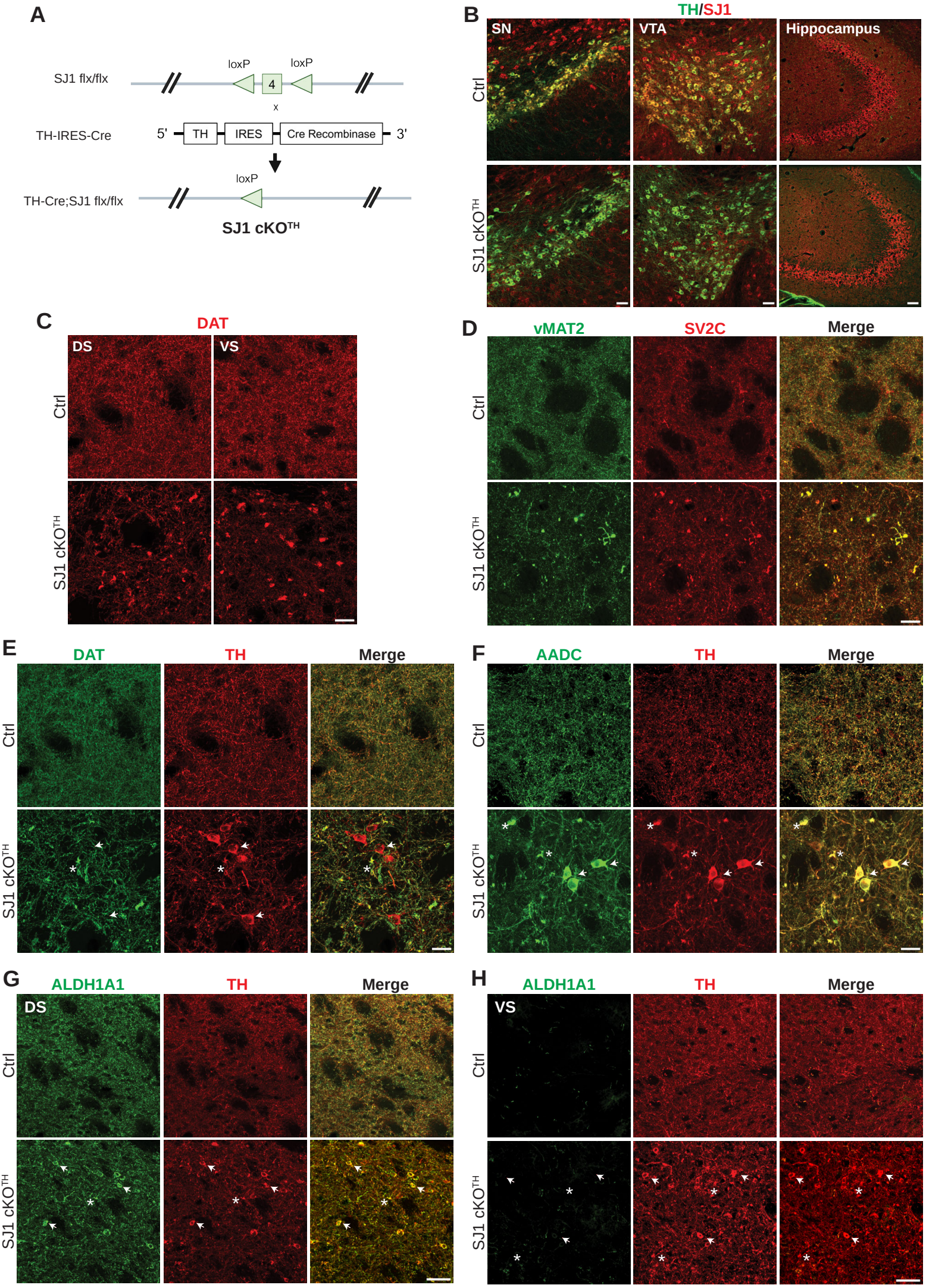
A
SJ1 flx/flx
loxP
loxP
4
x
TH-IRES-Cre
5'
TH
IRES
Cre Recombinase
3'
loxP
TH-Cre;SJ1 flx/flx
SJ1 cKO^TH
B
TH/SJ1
SN
VTA
Hippocampus
Ctrl
SJ1 cKO^TH
C
DAT
DS
VS
Ctrl
SJ1 cKO^TH
D
vMAT2
SV2C
Merge
Ctrl
SJ1 cKO^TH
E
DAT
TH
Merge
Ctrl
SJ1 cKO^TH
F
AADC
TH
Merge
Ctrl
SJ1 cKO^TH
G
ALDH1A1
TH
Merge
DS
Ctrl
SJ1 cKO^TH
H
ALDH1A1
TH
Merge
VS
Ctrl
SJ1 cKO^TH

Figure 5

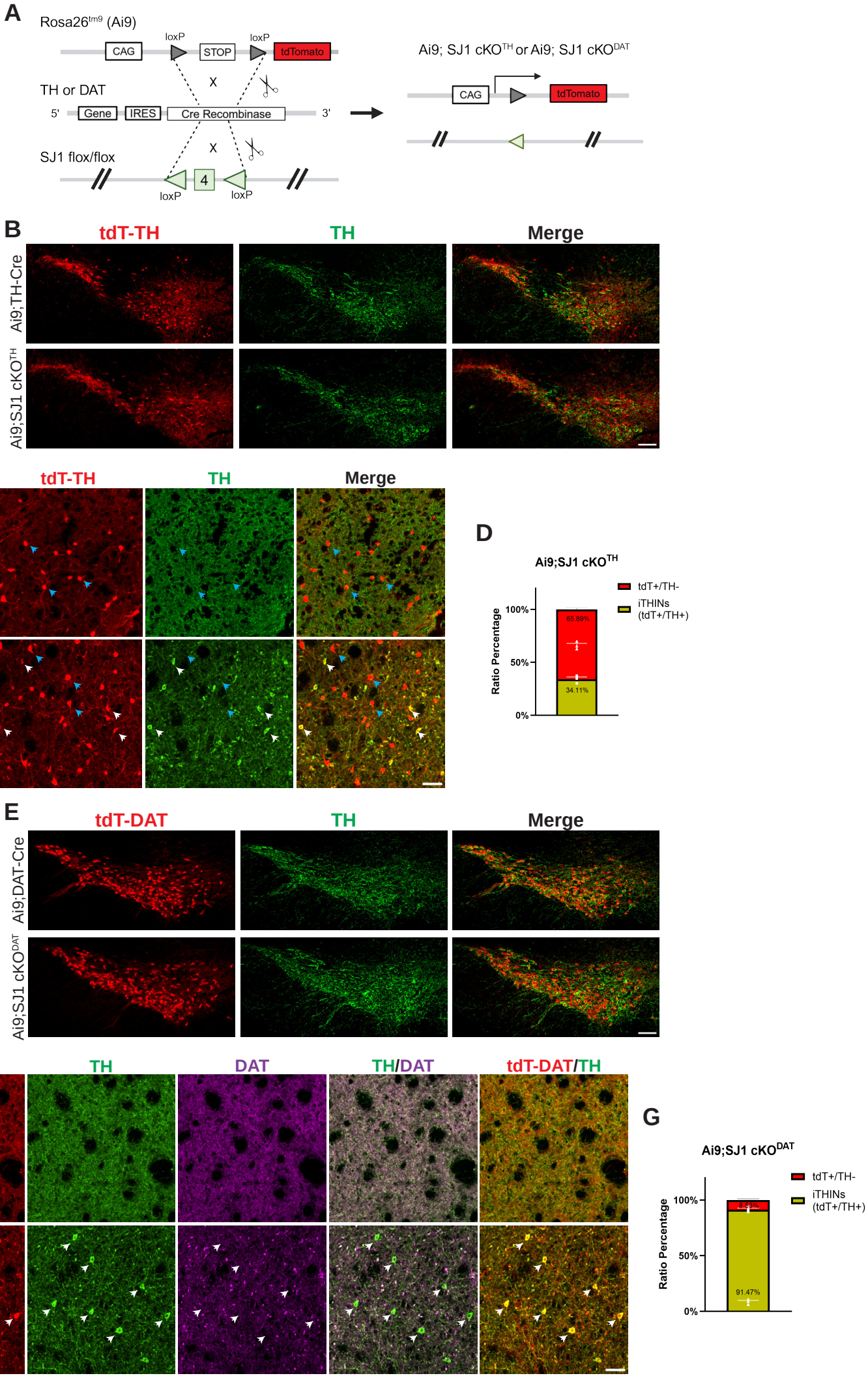
A
Rosa26tm9 (Ai9)
CAG
loxP
STOP
loxP
tdTomato
TH or DAT
5'
Gene
IRES
Cre Recombinase
3'
SJ1 flox/flox
loxP
4
loxP
Ai9; SJ1 cKOTH or Ai9; SJ1 cKODAT
CAG
tdTomato
B
tdT-TH
TH
Merge
Ai9;TH-Cre
Ai9;SJ1 cKOTH
C
tdT-TH
TH
Merge
Ai9;TH-Cre
Ai9;SJ1 cKOTH
D
Ai9;SJ1 cKOTH
tdT+/TH-
iTHINs (tdT+/TH+)
Ratio Percentage
100%
50%
0%
65.89%
34.11%
E
tdT-DAT
TH
Merge
Ai9;DAT-Cre
Ai9;SJ1 cKODAT
F
tdT-DAT
TH
DAT
TH/DAT
tdT-DAT/TH
Ai9; DAT-Cre
Ai9;SJ1 cKODAT
G
Ai9;SJ1 cKODAT
tdT+/TH-
iTHINs (tdT+/TH+)
Ratio Percentage
100%
50%
0%
91.47%

Figure 6

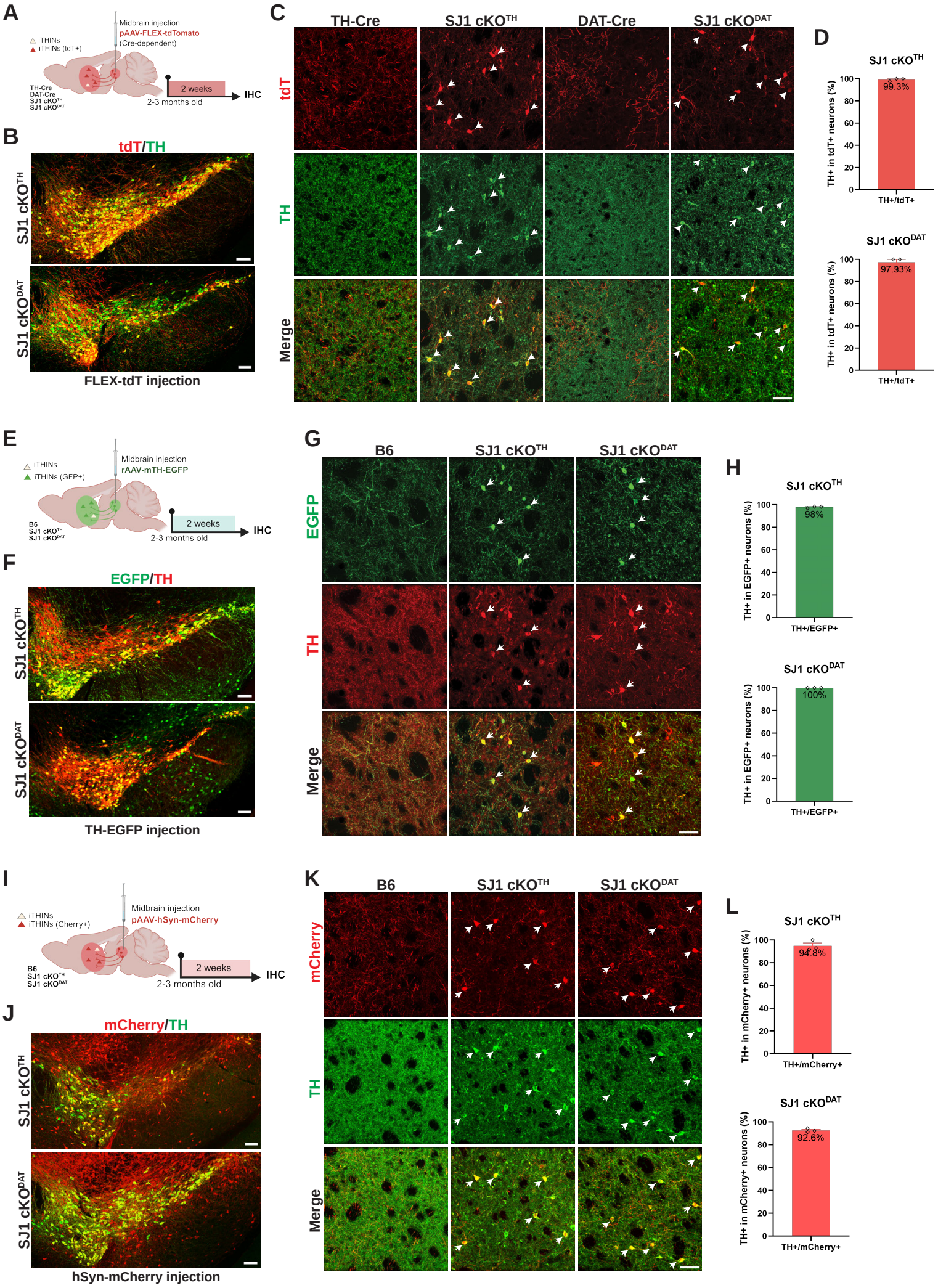
A
Midbrain injection
pAAV-FLEX-tdTomato
(Cre-dependent)
iTHINs
iTHINs (tdT+)
TH-Cre
DAT-Cre
SJ1 cKO^TH
SJ1 cKO^DAT
2 weeks
2-3 months old
IHC
B
tdT/TH
SJ1 cKO^TH
SJ1 cKO^DAT
FLEX-tdT injection
C
TH-Cre
SJ1 cKO^TH
DAT-Cre
SJ1 cKO^DAT
tdT
TH
Merge
D
SJ1 cKO^TH
99.3%
TH+ in tdT+ neurons (%)
TH+/tdT+
SJ1 cKO^DAT
97.33%
TH+ in tdT+ neurons (%)
TH+/tdT+
E
Midbrain injection
rAAV-mTH-EGFP
iTHINs
iTHINs (GFP+)
B6
SJ1 cKO^TH
SJ1 cKO^DAT
2 weeks
2-3 months old
IHC
F
EGFP/TH
SJ1 cKO^TH
SJ1 cKO^DAT
TH-EGFP injection
G
B6
SJ1 cKO^TH
SJ1 cKO^DAT
EGFP
TH
Merge
H
SJ1 cKO^TH
98%
TH+ in EGFP+ neurons (%)
TH+/EGFP+
SJ1 cKO^DAT
100%
TH+ in EGFP+ neurons (%)
TH+/EGFP+
I
Midbrain injection
pAAV-hSyn-mCherry
iTHINs
iTHINs (Cherry+)
B6
SJ1 cKO^TH
SJ1 cKO^DAT
2 weeks
2-3 months old
IHC
J
mCherry/TH
SJ1 cKO^TH
SJ1 cKO^DAT
hSyn-mCherry injection
K
B6
SJ1 cKO^TH
SJ1 cKO^DAT
mCherry
TH
Merge
L
SJ1 cKO^TH
94.8%
TH+ in mCherry+ neurons (%)
TH+/mCherry+
SJ1 cKO^DAT
92.6%
TH+ in mCherry+ neurons (%)
TH+/mCherry+

Figure 7

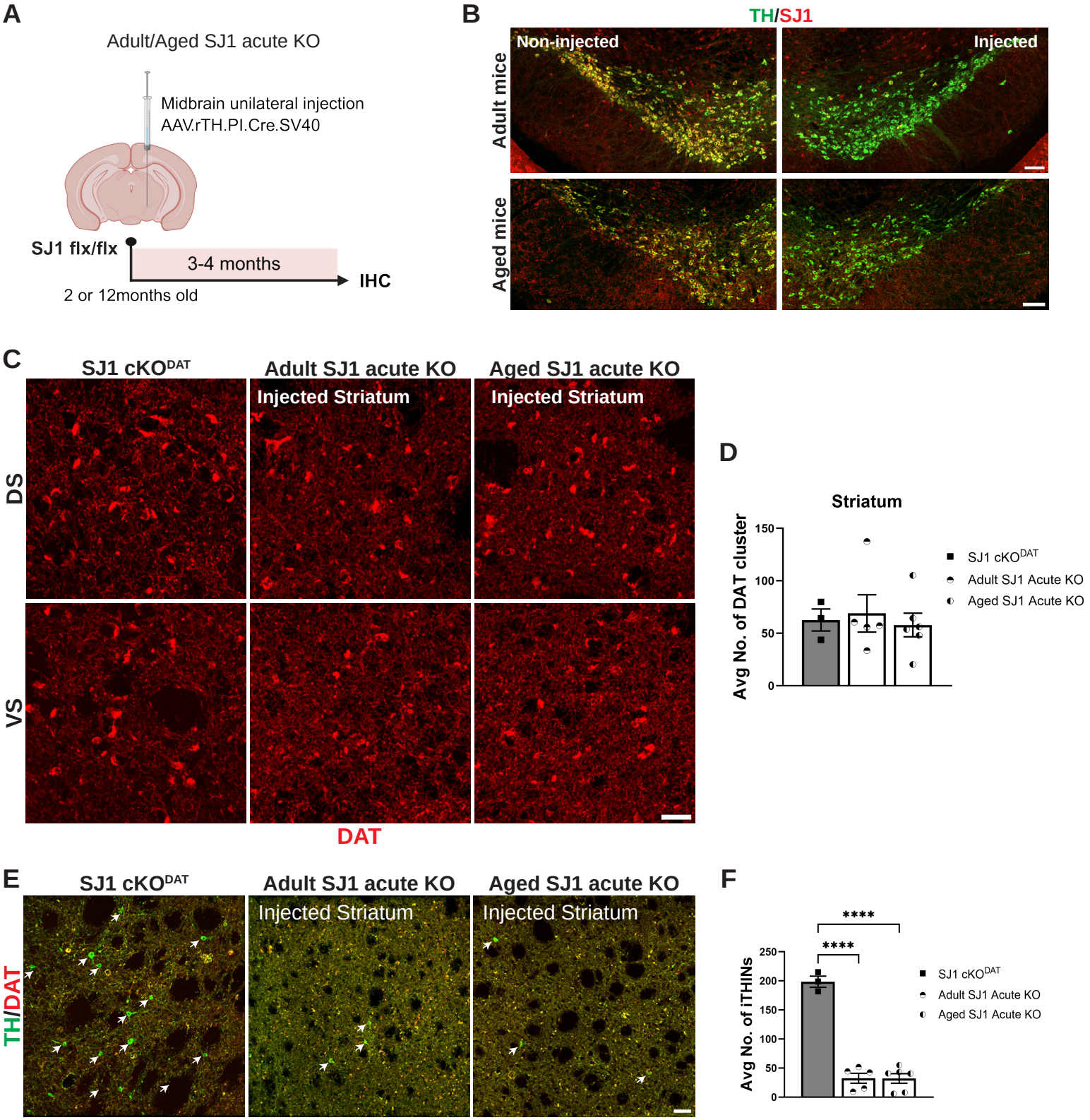
A
Adult/Aged SJ1 acute KO
Midbrain unilateral injection
AAV.rTH.PI.Cre.SV40
SJ1 flx/flx
3-4 months
IHC
2 or 12months old
B
TH/SJ1
Non-injected
Injected
Adult mice
Aged mice
C
SJ1 cKO^DAT
Adult SJ1 acute KO
Aged SJ1 acute KO
Injected Striatum
Injected Striatum
DS
VS
DAT
D
Striatum
Avg No. of DAT cluster
150
100
50
0
SJ1 cKO^DAT
Adult SJ1 Acute KO
Aged SJ1 Acute KO
E
SJ1 cKO^DAT
Adult SJ1 acute KO
Aged SJ1 acute KO
Injected Striatum
Injected Striatum
TH/DAT
F
****
****
Avg No. of iTHINs
250
200
150
100
50
0
SJ1 cKO^DAT
Adult SJ1 Acute KO
Aged SJ1 Acute KO

Figure 8

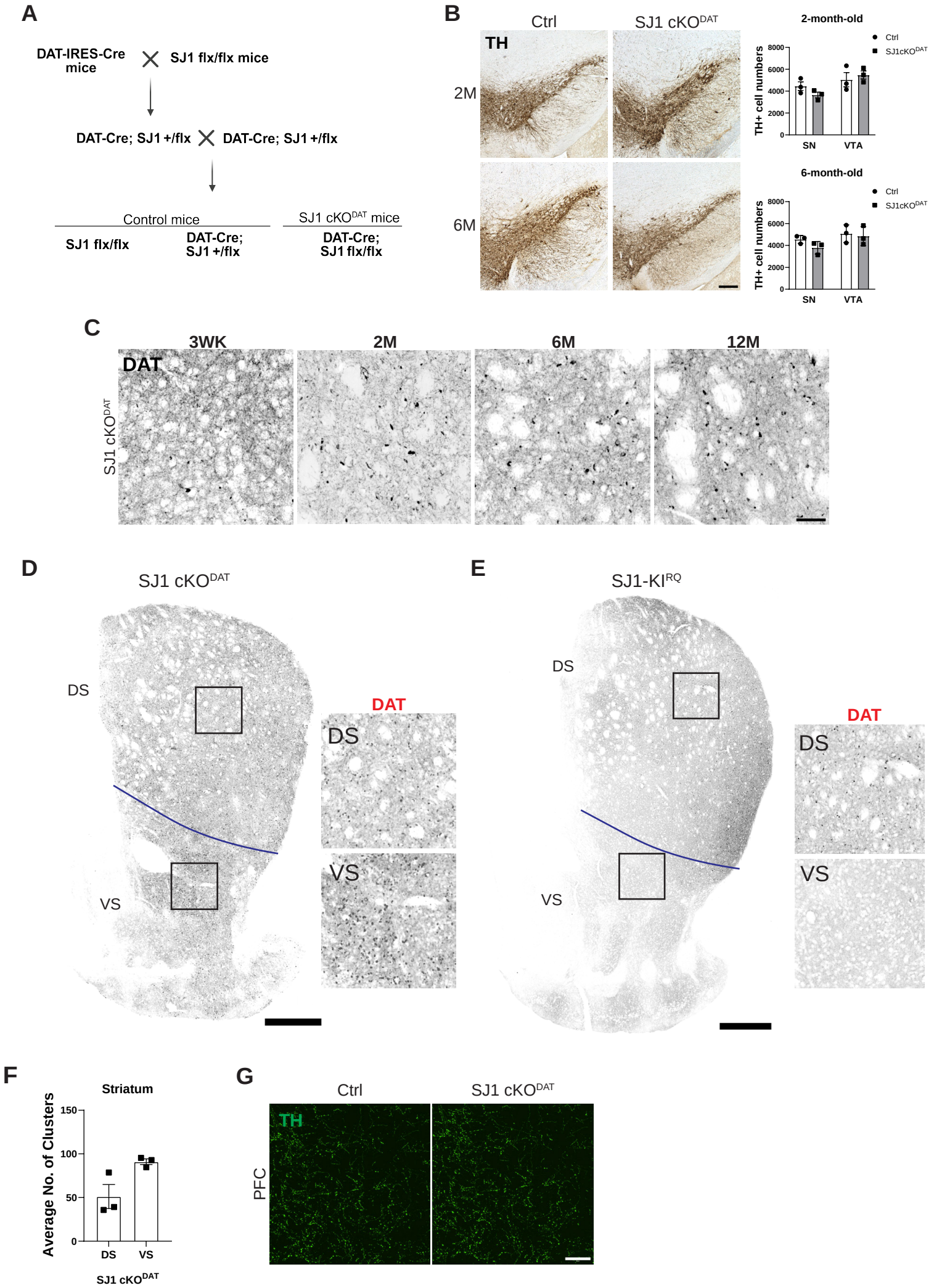

Supplementary Figure 1

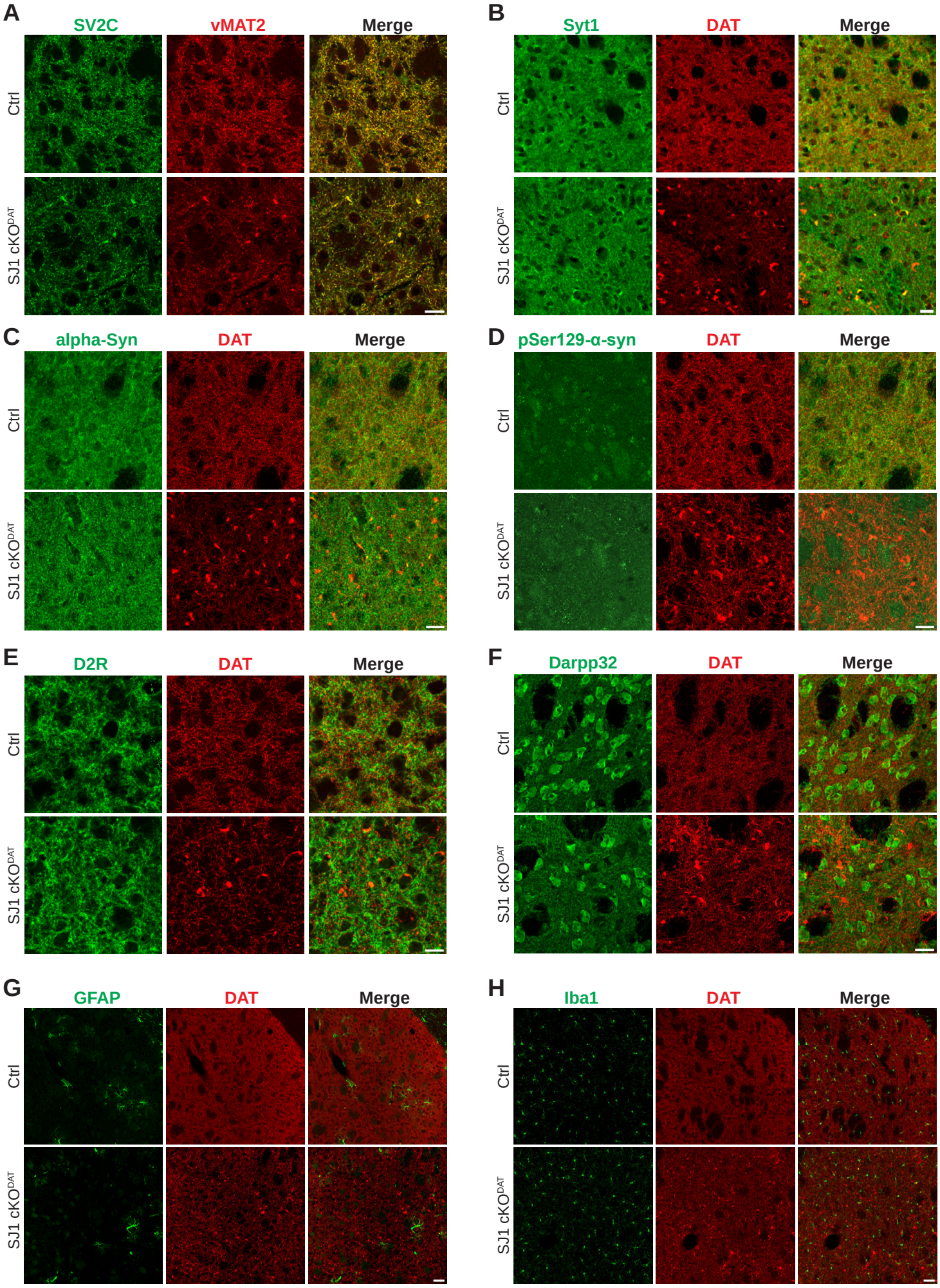

Supplementary Figure 2

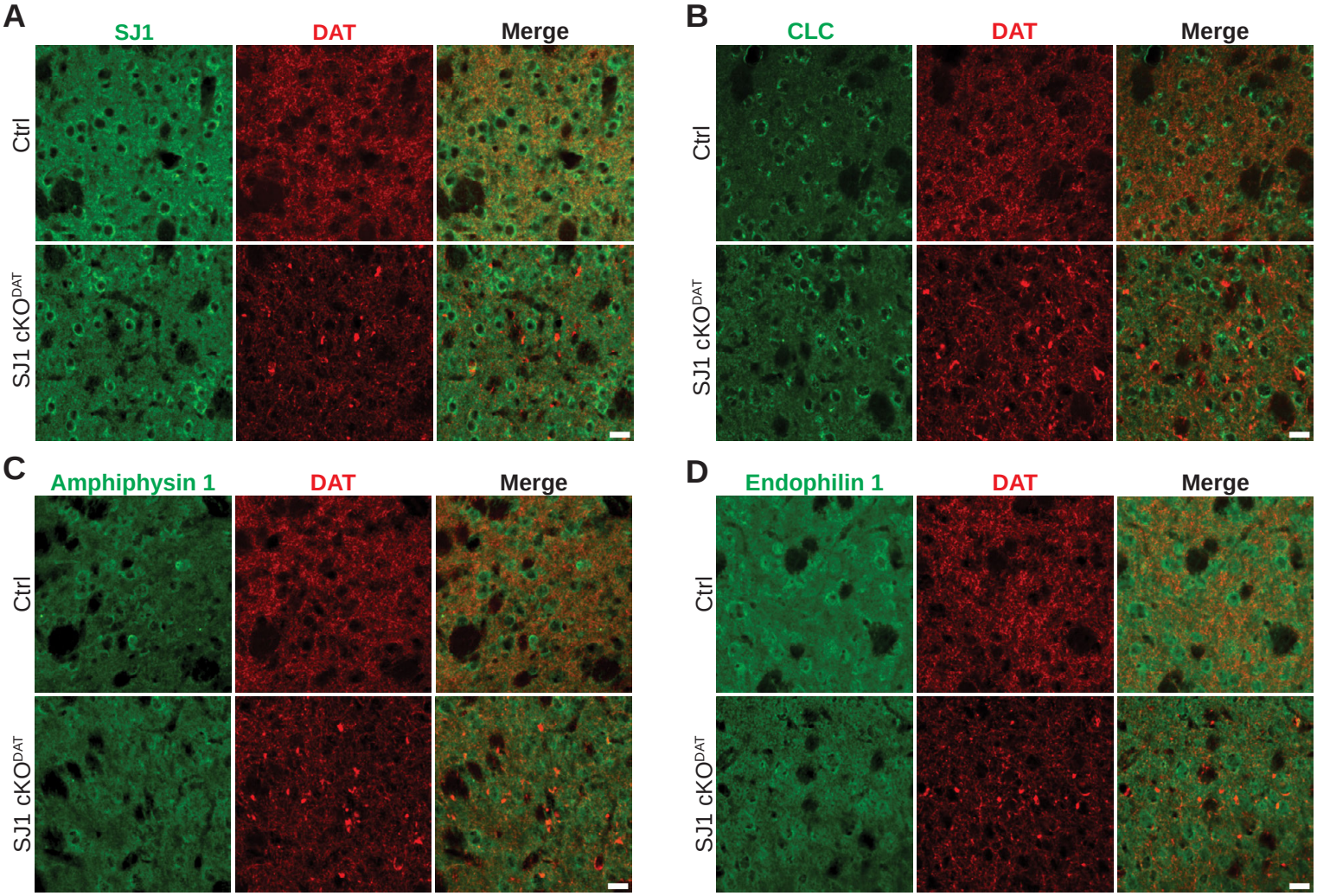

Supplementary Figure 3

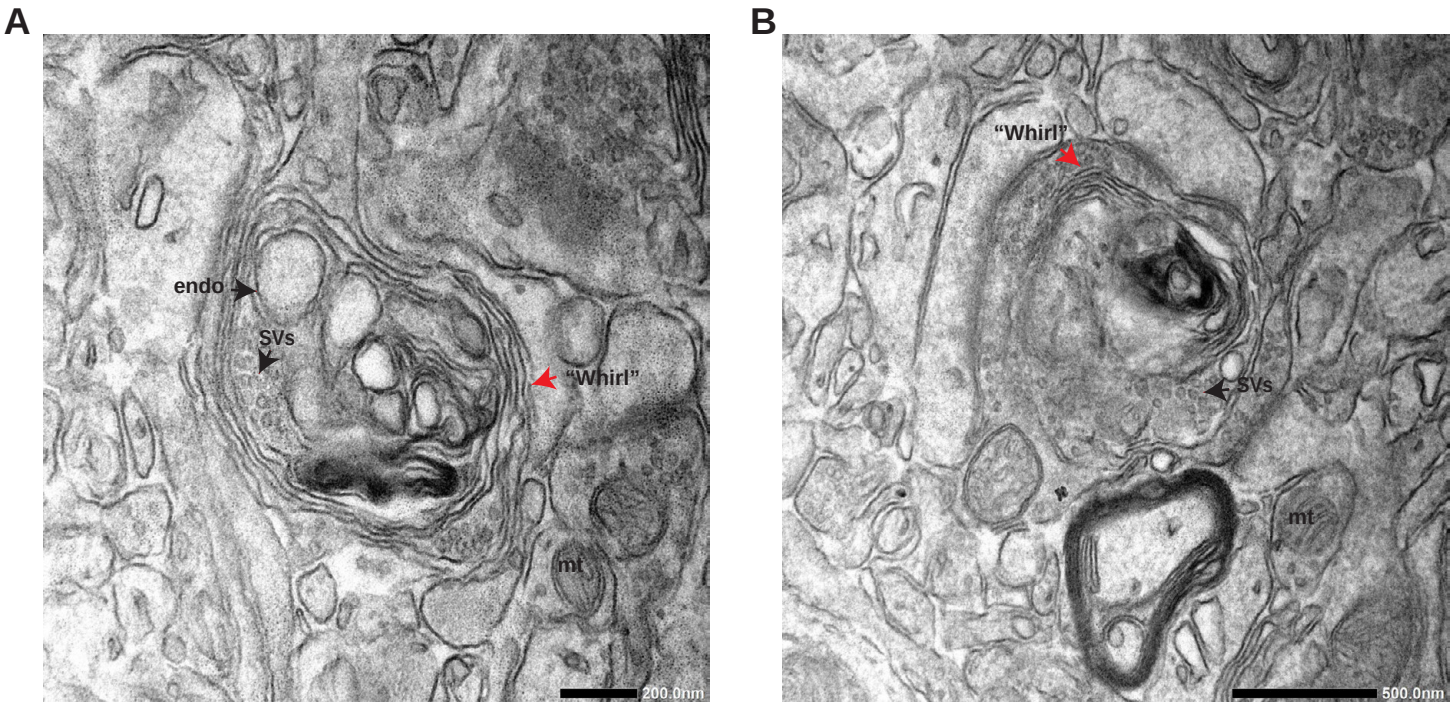

Supplementary Figure 4

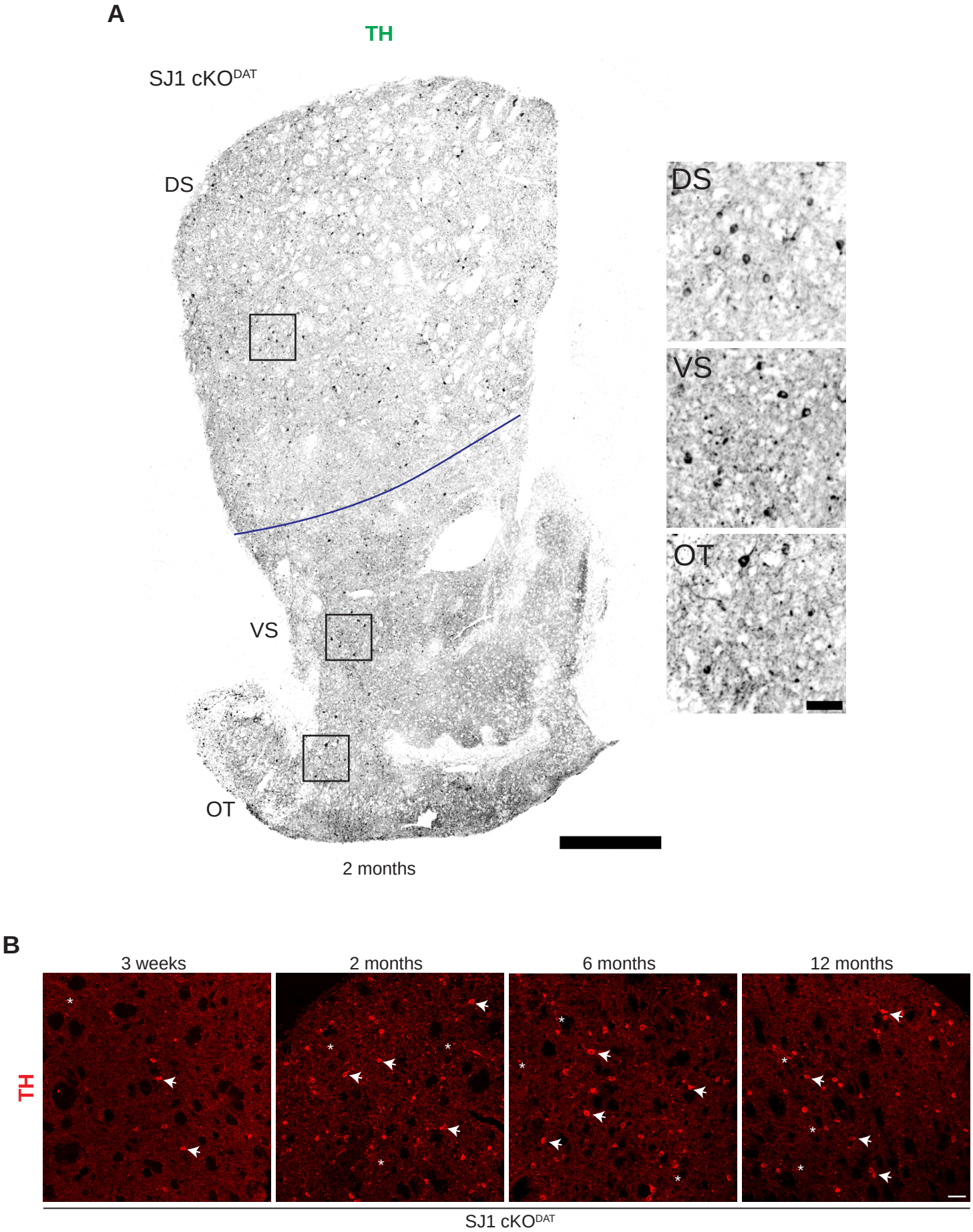

Supplementary Figure 5

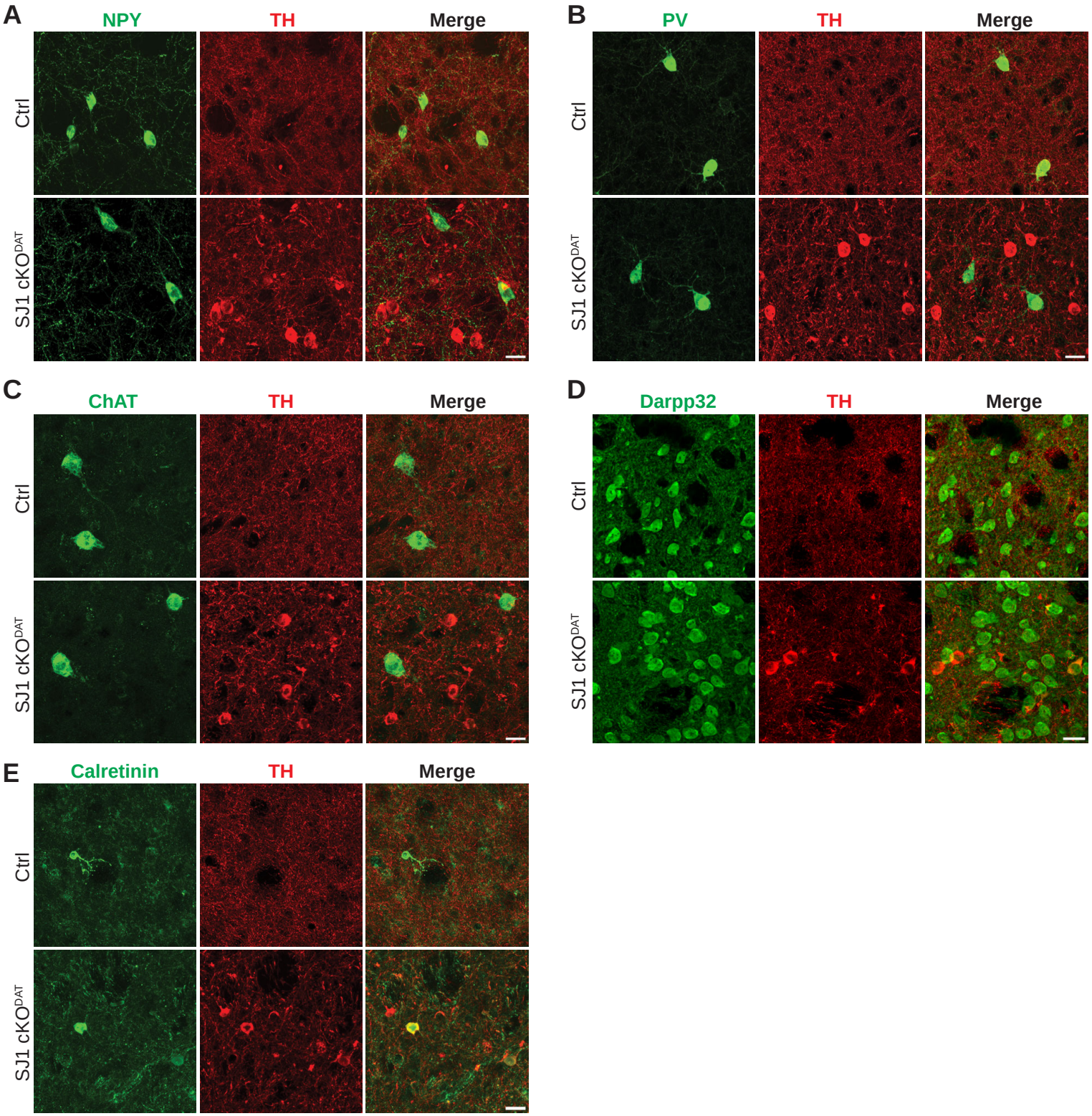

Supplementary Figure 6

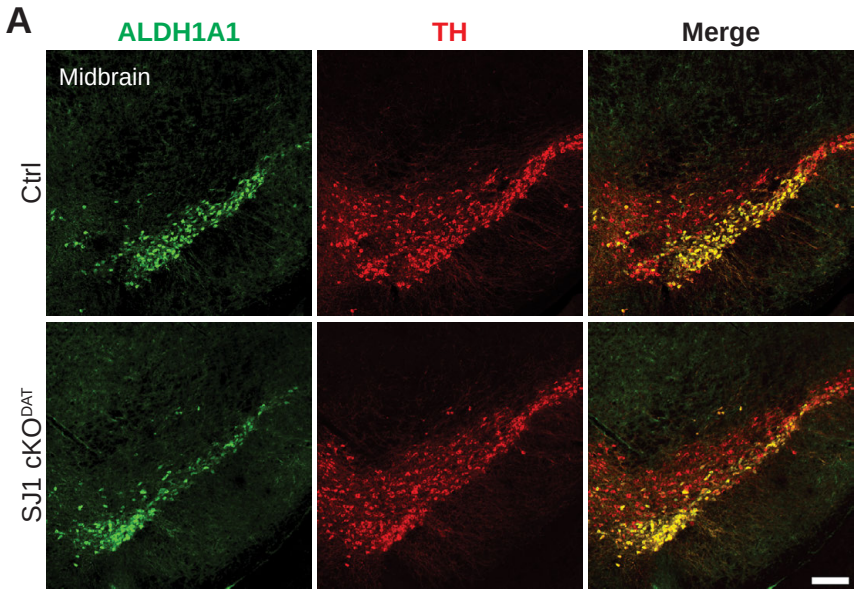

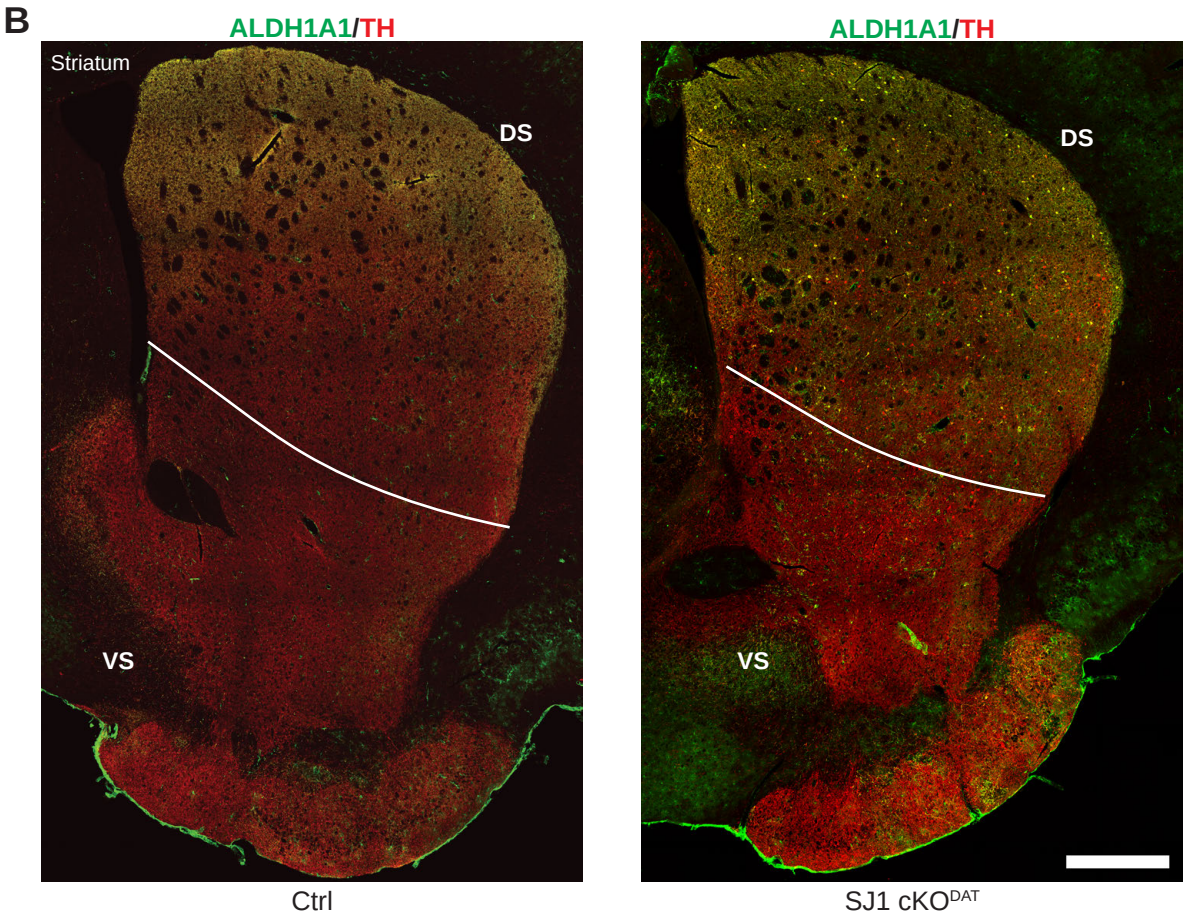

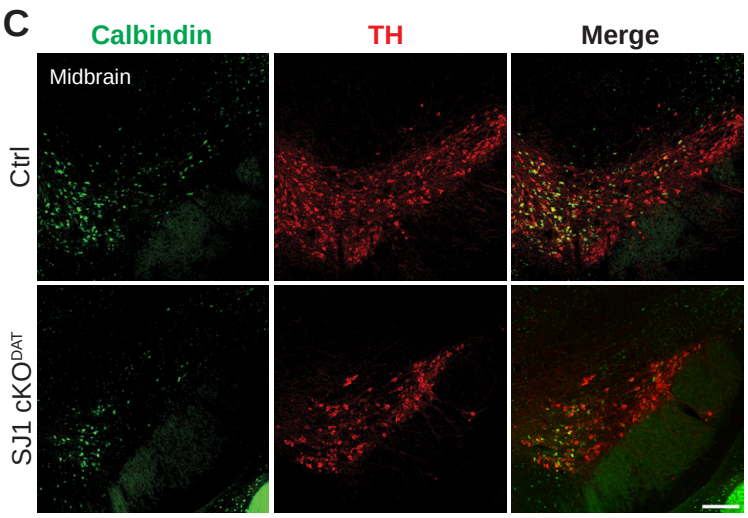

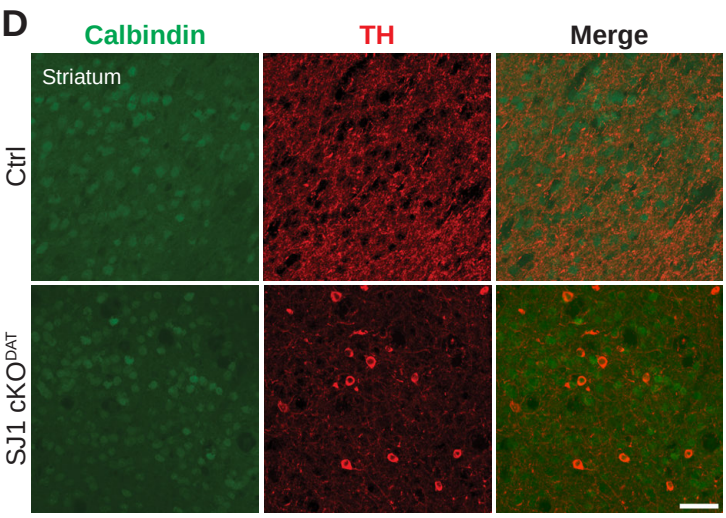

Supplementary Figure 7

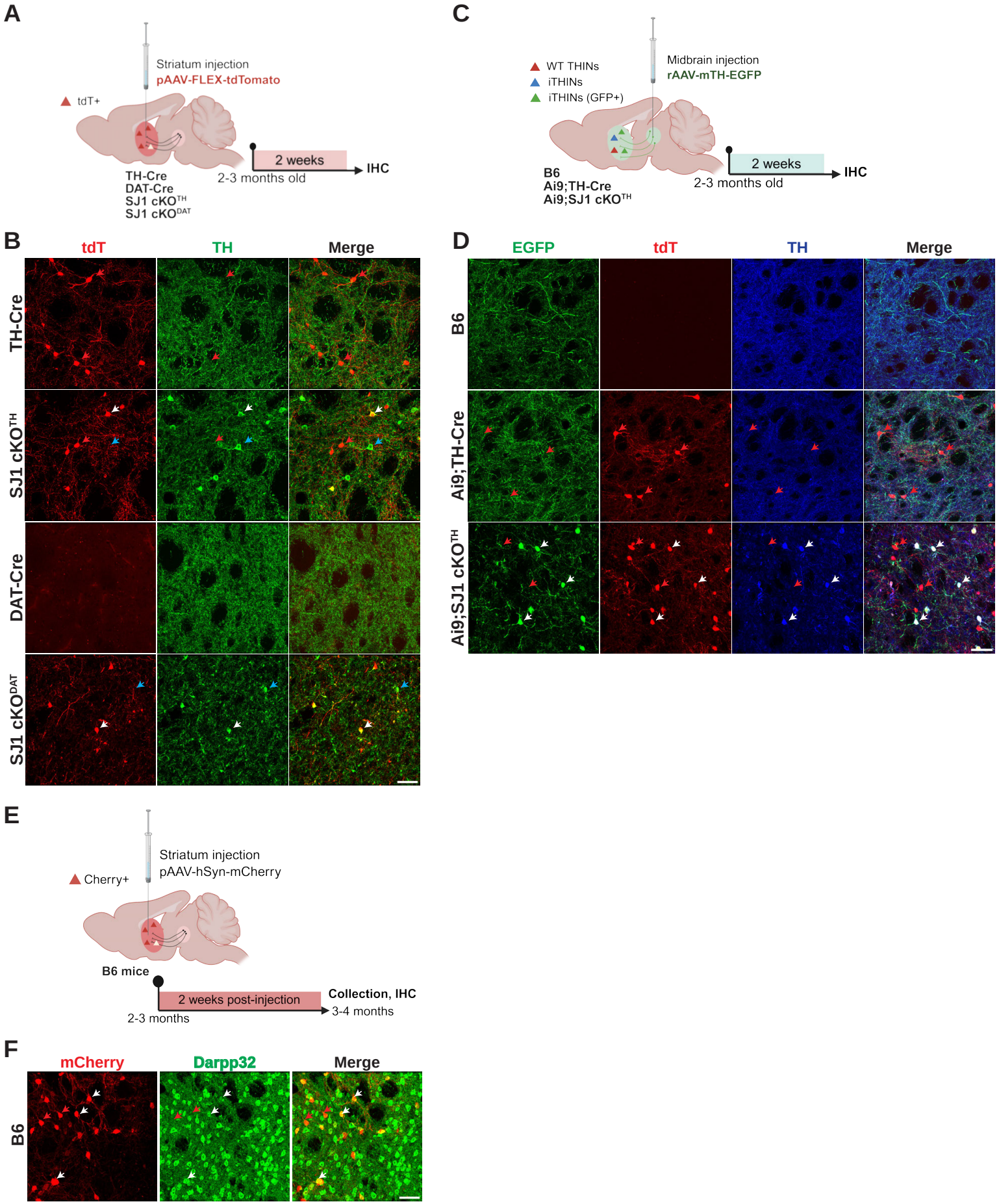

Supplementary Figure 8

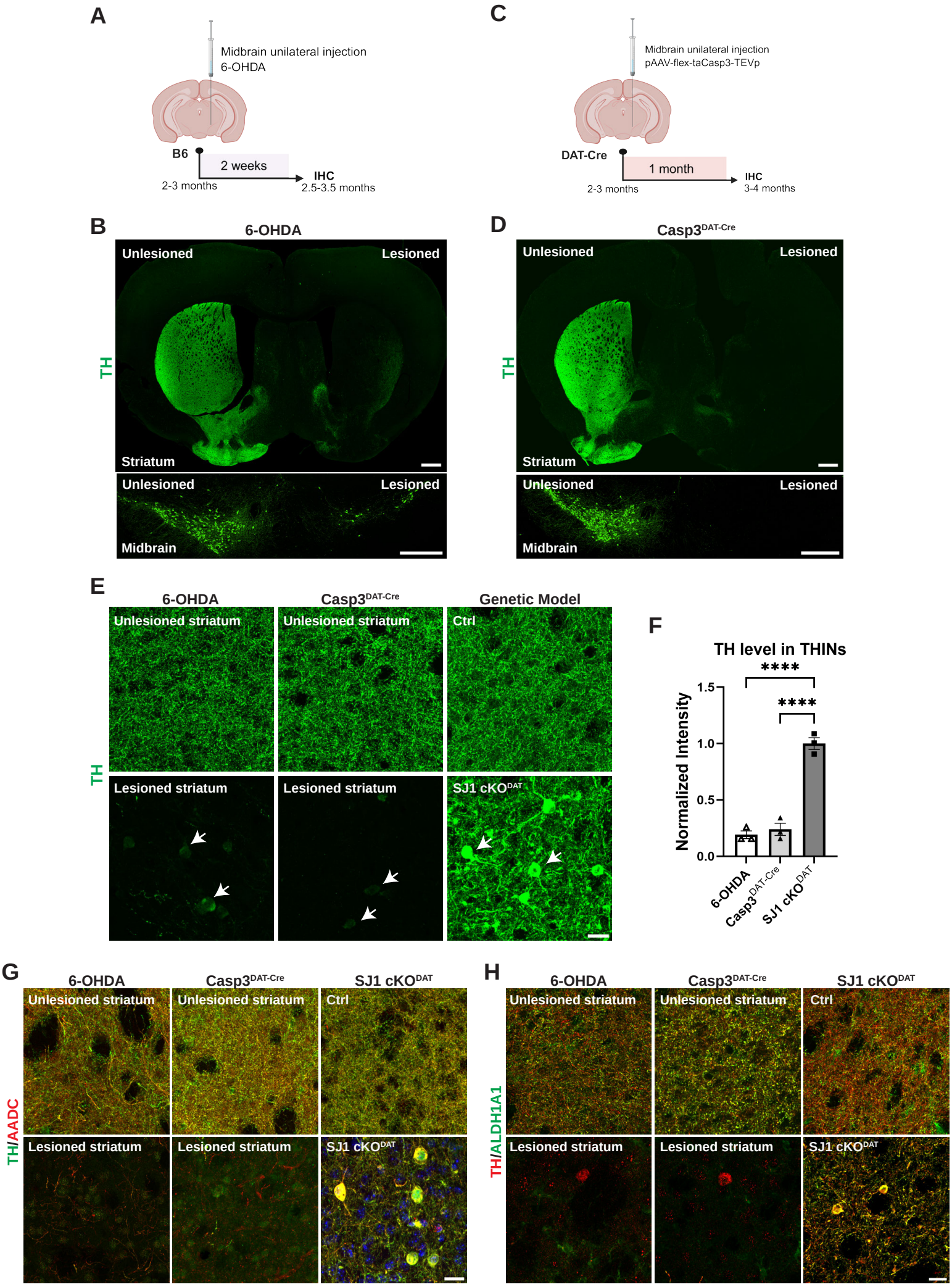

Supplementary Figure 9

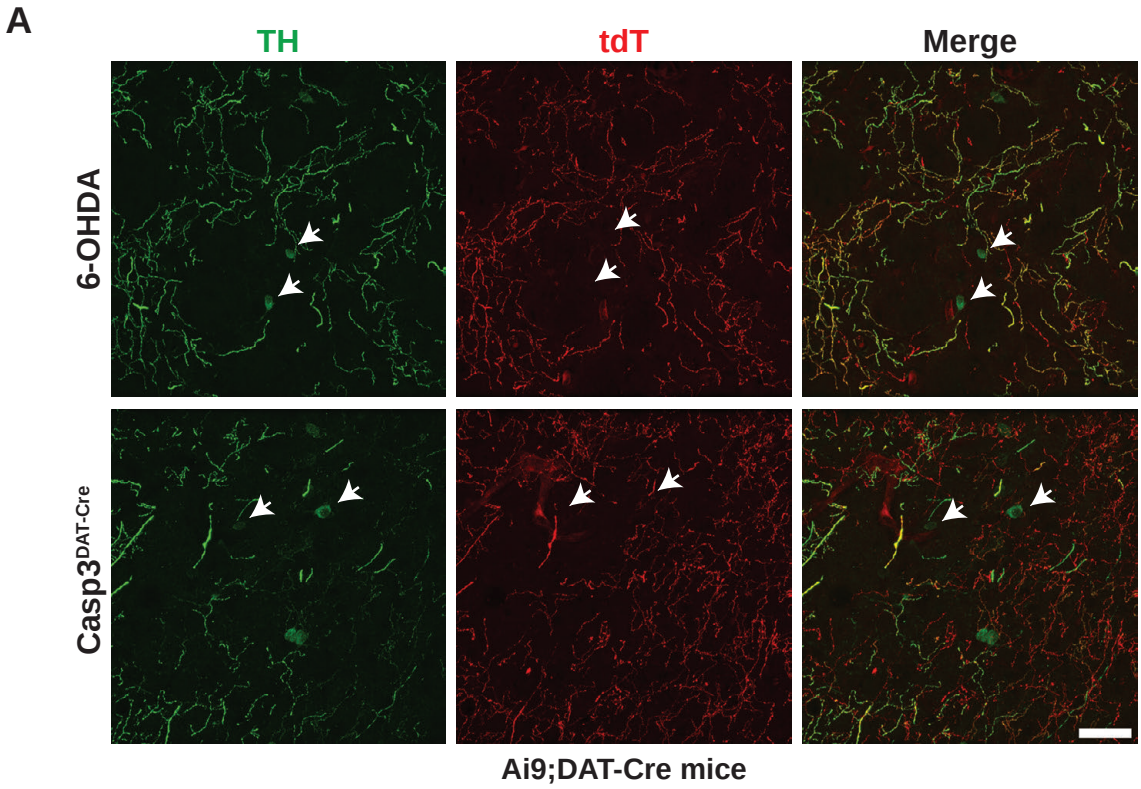

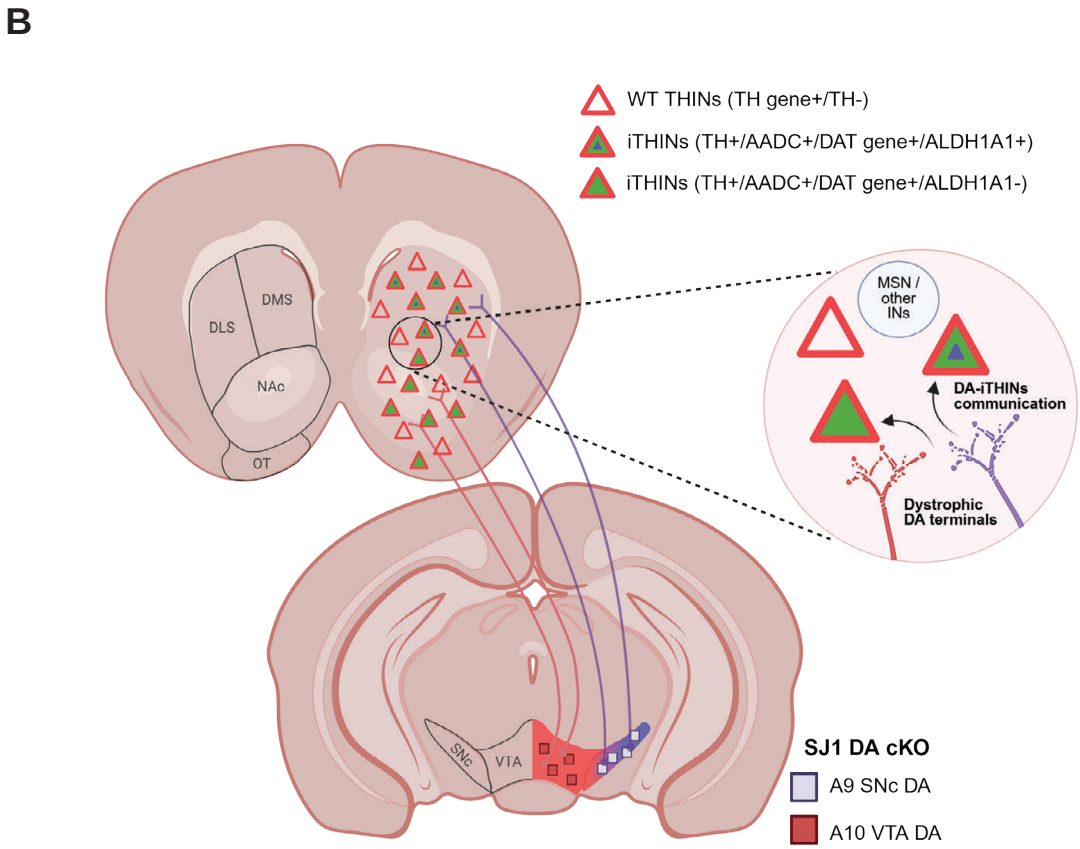

Supplementary Figure 10

A

AAV-TH-CRE injected in adult B6 mice

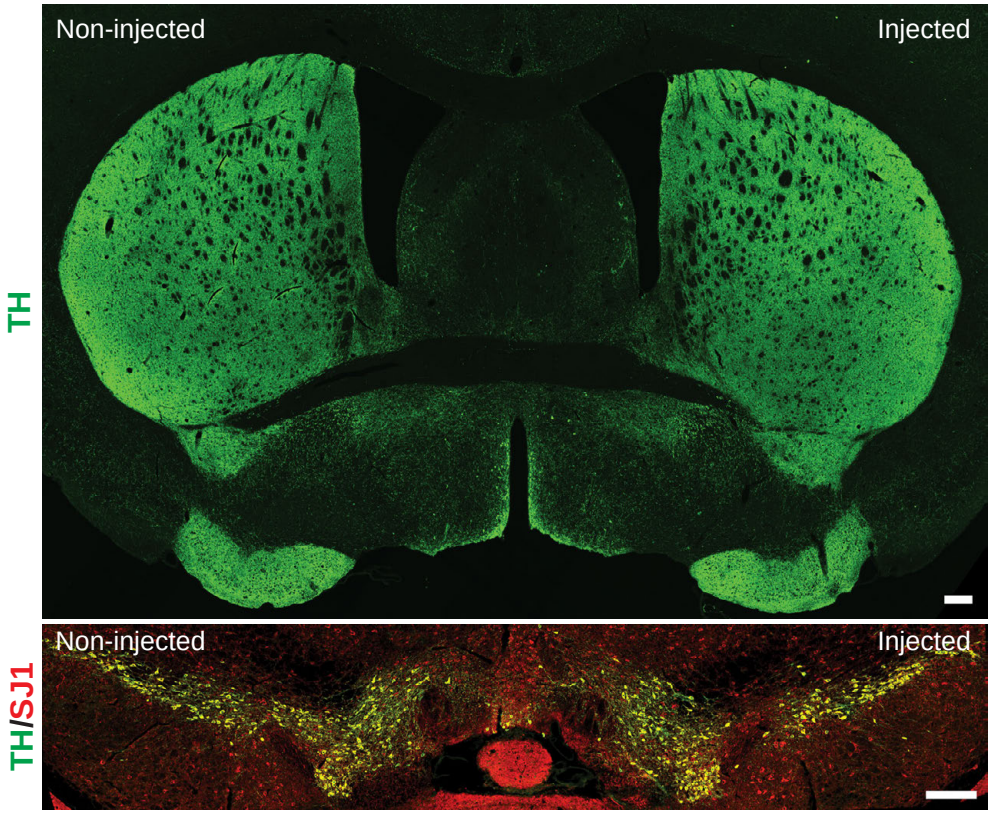

B

AAV-TH-CRE injected in aged B6 mice

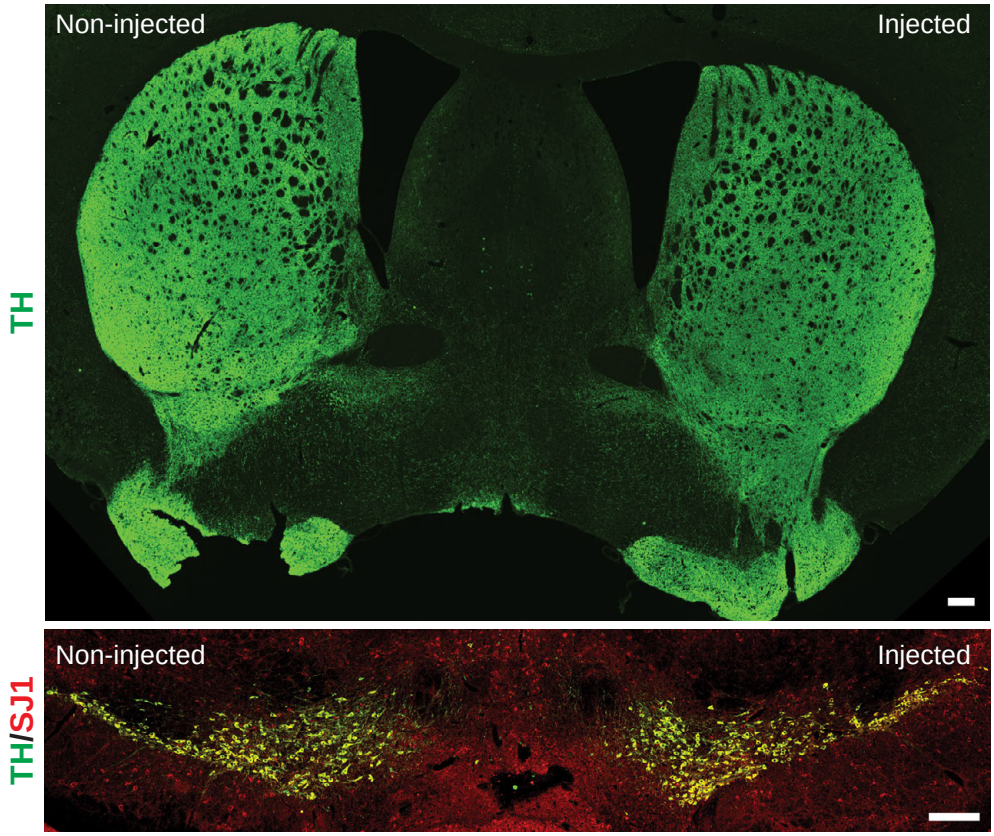

Supplementary Figure 11